Journal of Thermal Analysis and Calorimetry (2023) 148:7477–7500
https://doi.org/10.1007/s10973-023-12181-6

Check for updates

Effects of heat–light source on the thermal efficiency of flat plate solar collector when nanofluid is used as service fluid

Mahdiyeh Ahmadi[1] · **Majid Ahmadlouydarab**[2] · **Mohammadali Maysami**[1]

Received: 10 December 2022 / Accepted: 9 April 2023 / Published online: 1 May 2023

Abstract

The current experimental study aimed to investigate the effects of different nanofluids and heat–light sources on the thermal energy absorption of a laboratory-scale flat plate solar collector (FPSC). Water-based nanofluids containing Al_2O_3, SiO_2, and TiO_2 nanoparticles at a concentration of 0.2% were utilized as the service fluid in this study. The thermal behavior of the nanofluids in the FPSC was studied in two stages: heat absorption and heat retention periods. Both the heat absorption and retention periods were conducted for a duration of either 120 or 240 min. Distilled water acted as operating fluid circulating inside the insulated tank and the collector tubing system. Tungsten heat, halogen pencil, infra-red, and mercury vapor lamps were considered as heat–light sources. Among different heat–light sources considered, the collector utilizing a tungsten heat lamp demonstrated the highest thermal efficiency. For this lamp, the efficiencies for 120 min heat absorption were 67.37% for Al_2O_3, 66.21% for SiO_2, 64.64% for TiO_2 nanofluids, and 48.78% for base fluid. For the same lamp, during the 240 min heat absorption, these values were 44.72% for Al_2O_3, 43.42 for SiO_2, 42.26% for TiO_2 nanofluids, and 37.17% for base fluid. Aside from these, results showed that the thermal efficiency of FPSC with insulation and without insulation was 23% and 20% for 0.2% TiO_2 nanofluid, respectively, when halogen pencil lamp was used. Finally, results of considering distilled water or distilled water containing 0.2%, 0.5%, and 1% SDS as service fluid indicated that the highest amount of heat transfer was related to the distilled water. Indeed, heat transfer decreased with increasing SDS content.

Keywords Flat plate solar collector · Energy absorption and retention · Thermal efficiency · Heat–light source · Nanofluids · SDS

List of symbols

- A_c Area of the collector surface
- C_p The specific heat capacity
- C_s The average crystalline particle
- F_R Heat removal factor
- G The average light intensity arrived to the collector surface
- K Dimensionless crystal shape factor
- $\dot{m}$ The mass flow rate
- Q_t Total heat absorbed
- Q_{of} The amount of heat absorbed by operating fluid
- Q_s The amount of heat absorbed by service fluid
- Q_{cb} The amount of heat absorbed by collector body
- Q_{ct} The amount of heat absorbed by collector tubing
- Q_{wt} The amount of heat absorbed by water tank
- Q_L Lost heat
- T_o Outlet temperature
- T_i Inlet temperature
- T_a Ambient temperature
- U_L General loss coefficient of the solar collector

Greek symbols

- λ Wavelength of XRD
- β Peak width at half maximum height
- θ Different angle
- η Collector thermal efficiency

✉ Majid Ahmadlouydarab
mahmadlouydarab@tabrizu.ac.ir

[1] Department of Biosystems Engineering, Faculty of Agriculture, University of Tabriz, Tabriz, Iran

[2] Faculty of Chemical and Petroleum Engineering, University of Tabriz, Tabriz, Iran

Introduction

Due to environmental pollution and the disappearance of fossil fuel sources, the tendency to use renewable energy sources has increased. Solar thermal energy as one of the most important renewable sources is directly and indirectly available. Sun collectors are actually thermal converters that transform the energy of the sun into the internal energy of the collector's fluid agent. This equipment, with the absorption of radiant energy, transmits it into the operating fluid in the collector (usually air, water, or oil). The collected energy from the operating fluid can be used to directly heat daily consumption or stored water reservoirs [1]. Pandey and Chaurasiya in 2017 presented a comprehensive review of different methods for increasing the performance of flat plate solar collector (FPSCs) [2]. The advancements in nanotechnology have led to the development of high-performance nanostructured materials that possess the ability to absorb thermal energy and release it when necessary [3]. In 1995, Choi was the first researcher to use nanofluids to address the issue of nanofluids as a new heat transfer medium [4]. Nanofluids, due to the high potential for heat transfer, have been the subject of many recent studies [5]. Addition of nanoparticles to the base fluid suspension can drastically alter the optical properties of the fluid [6, 7]. The optical properties of a fluid strongly depend on the shape of the particles, the particle size, the optical properties of the base fluid, and the nanoparticles themselves [8]. Various materials such as aluminum [9], copper [10], and multi-wall carbon nanotubes [11–14] are added to different base fluids, and their properties are identified for improving the heat transfer efficiency. Wang and Mujumdar emphasized that the homogeneous suspension of nanoparticles in the base fluid significantly alters the heat transfer properties of the suspension [15]. Masuda et al. made alumina and titania nanofluids with a weighted percentage of 4.3 mass% and showed that thermal conductivity of the solution increased by 32% and 11%, respectively [16]. Grimm dispersed alumina nanoparticles with a diameter of 1–80 nm in the fluid and concluded that for the fluid 0.5–5% by mass, a 100% increase in thermal conductivity is observed [17]. Veeranna and Lakshmi briefly described the fabrication method of Al_2O_3 nanofluid and the factors affecting the improvement in thermal conductivity [18]. They reported that Al_2O_3 nanofluid had a higher potential for increased heat transfer and was suitable for practical heat transfer applications. On the other hand, the use of copper nanoparticles improves thermal conductivity and very small concentrations of particles lead to a major increase in the thermal conductivity of the oil [19]. In another study, Taylor studied nanofluid optical properties [20]. In Taylor's research, nanoparticles that were combination of water and graphite, aluminum, copper, silver, and titanium dioxide nanoparticles were used as an absorption environment. According to the results, more than 95% of the incoming sunlight could be absorbed.

Al_2O_3/water nanofluid due to high thermal conductivity, low density, and cheap price is the most common nanoparticle used in FPSCs among other metal oxides [21]. The use of nanofluid makes fast heat transfer and high heat absorption [22–24]. Eastman reported that under laboratory conditions, the addition of Cu nanoparticles into water at different concentrations significantly improves heat transfer behavior [25]. His results indicated that by adding 4% volume of heat transfer nanoparticles, heat transfer increased by up to 50%. He et al. analyzed the efficiency of a FPSC when using Cu–H_2O nanofluid and found that the thermal efficiency was increased by 23.8% in comparison with the FPSC using water. Solar energy absorption experiments show that Cu-H_2O nanofluid has good absorption for solar energy and can effectively increase the thermal effectiveness of FPSC [26].

Effects of nanoparticles heat transfer coefficients also have been studied [27]. For example, the effect of Al_2O_3 nanoparticles was investigated in the forced heat transfer coefficient and indicated that at 0.3% concentration, the heat transfer coefficient increased by 8% [28]. Moreover, Xie et al. investigated the heat transfer coefficient in laminar flow of four nanofluids including particles of aluminum oxide, titanium oxide, zinc oxide, and magnesium oxide in the water-ethylene glycol base fluid [29]. The results showed the heat transfer coefficient of nanofluid containing magnesium oxide nanoparticles increased up to 252% in the Reynolds number of 1000. Other nanofluids also had a heat transfer coefficient more than the base fluid.

Thermal conductivity of fluids can be improved by optimally increasing the surfactant. When sodium dodecyl benzene sulfonate (SDBS) surfactant is added to a fluid, the thermal conductivity of the aqueous solution becomes more than that of pure water [30]. The use of nanofluids with surfactant is a better method among other techniques in terms of dispersion effect and thermal conductivity. Studies have shown that adding surfactant to a nanofluid containing alumina nanoparticles and pure water has a positive effect on FPSC functionality [31].

It has been shown that water is the best solar energy absorbance among four fluids including water, ethylene glycol, propylene glycol, and therminol VP-1, but still a weak absorbent which only absorbs 13% of energy [32].

As mentioned, in recent years, nanofluids have created greater potential in many fields, such as solar collectors and solar thermal energy storage [33]. Muhammad et al. examined nanofluid applications in vacuum tube and FPSC for efficiency, economic, and environmental considerations [34]. They concluded that nanofluids are a better alternative to conventional fluids. Experimental results have indicated that in radiators used by conventional cooling fluids, in order to increase the temperature in heat transfer, the power to pump fluid should be about 10 times more [35]. However, if the nanofluid is used in these systems (assuming 3 times higher thermal conductivity coefficient) without increasing in the cost of pumping, the heat transfer intensity increases 2 times. According to another study, the researchers concluded that high densities and low specific heat of nanoparticles lead to higher thermal efficiencies [36]. Therefore, a smaller solar collector that operates using nanofluids can be produced, reducing the mass, energy, and production cost of the collector. It can also reduce the area of the solar collector.

Kameya and Hanamura reported an increase in solar radiation absorption when using nanoparticle suspensions [37]. They investigated the radiation absorption properties of a suspension with nickel nanoparticles and concluded that the absorption coefficient of the nanoparticle suspension for visible wavelengths close to infrared was much higher than the base fluid. Han et al. examined photothermal properties, optical properties, biological behaviors, and thermal conductivity of black carbon nanofluid [38]. Their experiments showed that nanoparticles had better solar energy absorption properties. Hordy et al. examined the optical characteristics of MWCNT nanofluids [39]. The results showed that in most solar spectra, the absorption value was high and the ability to absorb about 100% of solar energy was available.

Rajput et al. carried out an experimental study to examine effects of using Al_2O_3/distilled water on the efficiency and functionality of a FPSC [40]. The results showed that nanoscale with a concentration of 0.3% showed a maximum increase in yield, 21.32%. Zamzamian et al. used Cu/EG nanofluid, and studied its effects as operating fluid on the efficiency of the FPSC. The efficiency of the FPSC increased by using Cu/EG nanofluids [41]. In recent years, Kilic et al. have also experimentally investigated the effect of using TiO_2/water nanofluid on the performance of a FPSC. They reported that the use of titania nanofluids in solar collectors performed better than pure water. The highest instantaneous efficiency for titania nanofluid was 48.67% while this value was 36.20% for pure water [42]. Aside from effects of surfactants, nanoparticle type, and its volume percentage, exergy analyses of FPSC have been investigated. For example, in an experimental study, using water, alumina nanofluid, and oxidant nanofluid as the operating fluid in a FPSC exergy analyses was investigated [43]. When 0.01% alumina nanofluid was used, the highest efficiency of 77.5% which was 21.9% higher than water's efficiency was obtained.

In an innovative experimental study in 2020, Ahmadlouydarab et al. investigated the effects of using nanofluid as a service fluid on improving heat absorption and the efficiency of a FPSC [44]. They experimentally used water-based TiO_2 nanofluid and infrared lamp as a light–heat source. Authors concluded that using nanofluid as a service fluid at a concentration of 5% increases the collector efficiency by 49%.

Qi et al. studied the optical constants and properties of paraffin suspension containing TiO_2 nanoparticles. Their results indicated that the concentration was the main factor affecting the absorption index and absorption coefficient while the particle size of TiO_2 was secondary factor [45].

Nanoparticles show unique heat transfer properties due to their small size and large surface area-to-volume ratio. These properties can result in enhancements in thermal conductivity, capacity, and diffusivity of the nanofluids compared to the base fluids. This is because when nanoparticles are suspended within a fluid, they interact with the surrounding molecules and create disturbances that alter the overall transport properties of the mixture. Additionally, the high surface area of nanoparticles allows for greater absorption of thermal energy, which can be released efficiently when necessary. Nanoparticles have also shown to exhibit other interesting thermal phenomena such as enhanced boiling heat transfer and critical heat flux [46]. These properties make nanofluids an attractive option for improving the performance of heat transfer systems, including solar collectors. The thermal conductivity of nanoparticles is one of the most important properties that makes them attractive for use in nanofluids. Due to their small size and high surface area-to-volume ratio, nanoparticles can exhibit exceptional thermal conductivity compared to the base fluid. This can result in significant enhancements in the overall thermal conductivity of the nanofluid. The effect of nanoparticle concentration on the thermal conductivity of nanofluids has been extensively studied [47]. However, at higher concentrations, the thermal conductivity enhancement tends to saturate due to the formation of particle clusters or agglomerates, which decrease the effective surface area available for heat transfer. The type of nanoparticle used can also have a significant impact on the thermal conductivity enhancement, as different materials possess different thermal conductivities [48]. For example, metal-based nanoparticles generally exhibit higher thermal conductivities than oxide-based nanoparticles due to their metallic bonding structure.

Upman and Srivastava investigated the parameters affecting thermal conductivity enhancement in oxide nanofluids [49]. They found that nanofluids with a low concentration of nanoparticles exhibited significantly higher thermal conductivity than their corresponding base fluids. Additionally, the researchers identified several factors influencing the thermal conductivity enhancement of nanofluids, including the volume fraction of particles, type of base fluid, size and shape of nanoparticles, temperature, and type of nanoparticles used.

Rashmi et al. investigated the stability and thermal conductivity enhancement of carbon nanotube (CNT) nanofluid using Arabic gum (AG). Through their experimental study, they measured the effective thermal conductivity of aqueous CNT nanofluid at varying concentrations of both CNTs and AG. The findings indicated that an increase in CNT concentration led to a rise in effective thermal conductivity. However, AG did not have any effect on thermal conductivity enhancement of CNT nanofluid [50].

Table 1 summarizes some studies in which different types of nanofluids were utilized in solar systems over the last two decades.

Table 1 Applications of nanofluids in different solar systems used in recent decades

Investigator(s)	Year	Type of used particles	Findings	Reference nos.
Wang et al	1999	Al_2O_3, CuO	12% Improvement from 3 vol% Al2O3/water nanofluids	[51]
Phelan et al	2010	Carbon nanotubes, graphite, and silver	They demonstrate efficiency improvements of up to 5% in solar thermal collectors by utilizing nanofluids as the absorption mechanism	[52]
Sabaghan et al	2016	TiO_2, Silicon	Using nanofluid can improve the normalized efficiency by 27%	[53]
Amina et al	2016	Al_2O_3, Cu, Sic	They observed the thermal improvement with the addition of nanoparticles. Application of nanofluid as an internal HTF absorber with baffles improved the thermal performance	[54]
Gorji and Ranjbar	2017	Graphite, Magnetite, Silver/water	Nanofluid magnetite/water achieved the highest thermal and energy efficiency, with graphite and silver following	[55]
Aberoumand et al	2018	Ag	The results showed that using nanofluids for cooling of the PV/T system can enhance both the energy and exergy efficiencies of the system significantly	[56]
Chen et al	2020	Carbon nanotubes	The thermal performance of the solar water heater was determined to be 73% at a solar intensity of 1000 W m^{-2}	[57]
Parsa et al	2022	Various nanofluids	They concluded that nanofluid preparation method and its stability also play crucial roles on the performance of PVTs	[58]
Islam and Furuta	2022	Carbon nanotube	Applying CNT composites and CNT coatings in solar water purification devices and solar thermoelectric generation devices leads to a remarkable enhancement in the system's overall efficiency	[59]
Kazaz et al	2023	Water-based mono and hybrid nanofluids (Cu, Au, Al, Al_2O_3, Graphite)	Hybrid nanofluids can be considered as effective heat transfer fluids to increase the solar radiation absorbability, and subsequently, improve the efficiency and performance of the direct absorption solar collector	[60]
Meibodi et al	2016	Different types of nanofluids	In the last years, Nanofluids in solar thermal systems have been studied as a useful technique to increase the performance of solar collectors and make them durable and highly efficient systems	[61]
Said et al	2018			[62]
Gupta et al	2018			[63]
Ghodbane et al	2019			[64]
Ehyaei et al	2019			[65]

Overall, the literature shows that the use of nanofluids has been found to improve the thermal efficiency of solar collectors in most cases. One of the key factors that can significantly impact the efficiency of a flat plate solar collector is the type and quality of the heat and light source. The ability of the collector to convert solar radiation into usable thermal energy is directly influenced by the intensity, spectrum, and angle of incidence of the incoming sunlight [66]. Addressing these factors, particularly optimizing the heat–light source, can help improve the overall efficiency of an FPSC and make it more effective in generating renewable energy. Indeed, there are relatively few studies that have investigated the use of different types of heat and light sources in flat plate solar collectors (FPSCs). This is partly due to the fact that natural sunlight is the most commonly used source of heat and light for FPSCs, and it can be challenging to replicate the intensity and spectrum of sunlight using artificial sources. Although more research is needed in this area, exploring alternative heat and light sources for FPSCs could prove to be an important strategy for improving their overall efficiency and effectiveness in generating renewable energy.

The present study aims to achieve the following objectives: firstly, to evaluate the effects of various types of heat–light sources, including tungsten heat lamp, halogen pencil lamp, infrared lamp, and vapor mercury lamp, on the thermal efficiency of flat plate solar collectors. Secondly, we will investigate how the type of nanofluid used as a service fluid inside the collector affects the thermal performance

Table 2 Physical properties of nanoparticles claimed by companies

Nanoparticle	APS[a]	Purity/%	SSA[b]/m^2/g	Morphology	Color
Al_2O_3	30–40 nm	99.6	250	Powder	White
SiO_2	30 nm	99.8	150	Powder	White
TiO_2	< 25 nm	99.7	45–55	Powder	White

[a]Average Particle Size

[b]Specific Surface Area

Table 3 Equipment and devices used in the present study

No.	Name	Model/made of/company
1	Flat plate solar collector	Plexiglass "PMMA[a]"
2	Water tank	Plastic tank with a volume of 3 L
3	Water pump	AQ901
4	Board	Arduino Uno R3 boards with ATmega328P CPU
5	Temperature sensor	DS18B20 waterproof with stainless steel probe
6	Thermal insulation	Elastomeric foam-MAFLEX
7	Fiberglass	–
8	Tungsten heat lamp	150 W
9	Halogen pencil lamp	150 W
10	Infrared lamp	250 W
11	Mercury vapor lamp	250 W
12	Agitator	ALFA—HS860
13	Ultrasonic probe	Hielscher-UP400S
14	Viscometer	BROOKFIELD DV-II + Pro ± 1%
15	Pycnometer	PYREX 50 mL
16	Digital scales	Precisa—BJ 100 M, d = 0.001 g
17	Luxmeter	MASTECH MS6612
18	Scanning electron microscope	Tescan-MIRA 3
19	Infrared spectrometer	Tensor 27-Bruker
20	Differential scanning calorimeter	NETZSCH-DSC 200 F3 Maia
21	X-ray diffraction spectrometer	SIEMENS-D 5000, 40, 30, Source: Cu
22	DLS[b]	Nanotrac Wave

[a]Polymethyl meth Acrylate

[b]Dynamic light scattering

of the FPSC. Finally, we will explore the impact of thermal absorption and retention times on the efficiency of the FPSC.

Materials and experimental setup

Chemicals and equipment

The Al_2O_3 nanoparticles used in this study were obtained from Rayka Sanat Afrand (Rasa) company, while SiO_2, TiO_2 and sodium dodecyl sulfate (SDS) surfactant were procured from Merck company. Table 2 presents a summary of the physical properties of the nanoparticles utilized in the preparation of the nanofluids for this study. Table 3 presents a detailed list of the equipment and devices that were utilized for the preparation of nanofluids and subsequent experimental procedures in this study.

The equipment and devices used to prepare the nanofluids and perform the experiments are listed in Table 3.

Nanofluid preparation and stabilization

A two-step method was employed to produce 760 mL of each nanofluid. Distilled water was infused with Al_2O_3, SiO_2, and TiO_2 nanoparticles at a mass–volume percentage of 0.2. To ensure the stability of the nanofluid, solutions were supplemented with 0.1 of the nanofluid, solutions were supplementedwith 0.1 mass% SDS and 0.1 mass% xanthan gum. The nanofluid was mixed using a magnetic stirrer for one hour followed by subjecting the resulting sample to 40 min of ultrasonic waves using an ultrasonic device with a probe to ensure proper dispersion. The base fluid contained 0.1% SDS and 0.1% xanthan gum without any addition of nanoparticles. A scale with an accuracy of 0.0001 g was used to obtain precise measurements of mass. Note that the xanthan gum is used to stabilize the nanofluid in order to avoid particles agglomeration and/or sedimentation. To reduce the effects of the xanthan gum on the nanofluid/ base fluid behavior, the minimum amount of xanthan gum was used.

Nanofluid analyses

FESEM[1] was used to analyze the properties of the nanofluids, the dispersion behavior of the nanoparticles in the base fluid, the stability of the suspensions, and the agglomeration rate. Figures 1–3 show the field emission scanning electron

[1] Field emission scanning electron microscope.

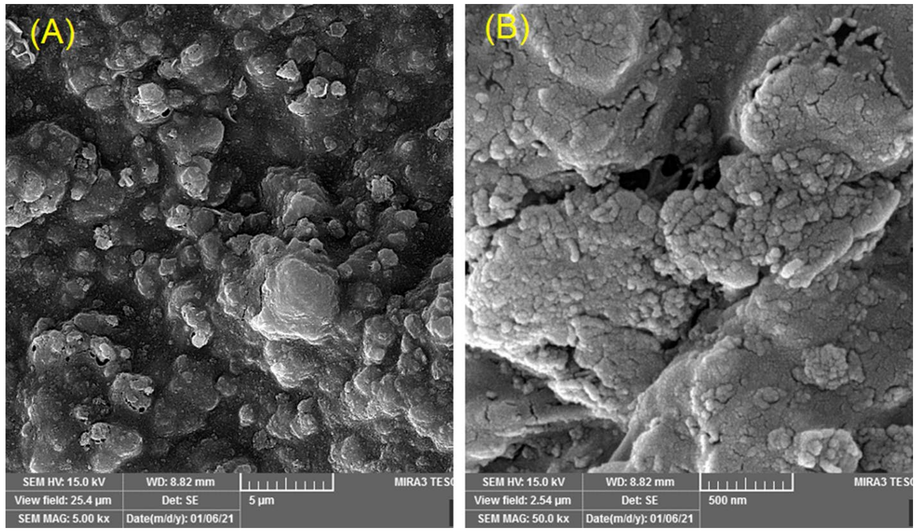

Fig. 1 FESEM images of alumina (Al_2O_3) nanoparticles. **A** Low magnification and **B** high magnification

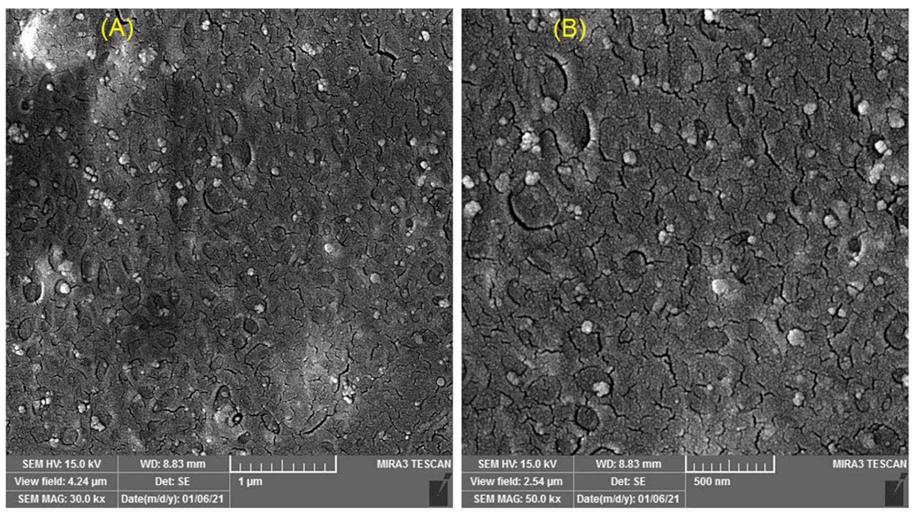

Fig. 2 FESEM images of silica (SiO_2) nanoparticles. **A** Low magnification and **B** high magnification

microscopy images of Al_2O_3, SiO_2 and TiO_2 nanoparticles. As shown in the figures, the agglomerated particles are not visible in the images, and the distribution of nanoparticles in the base fluid is homogeneous and uniform. Spherical morphology can also be identified. The average particle size in Al_2O_3, SiO_2, and TiO_2 nanofluids was 56 nm, 50 nm, and 47 nm, respectively.

Fourier transform infrared (FTIR) analysis was conducted in the range of 500–4000 cm^{-1} to investigate the properties of nanoparticles and assess the quality of the purchased materials. The X-ray diffraction (XRD) technique was employed to analyze and characterize the crystals present in the nanoparticles. By comparing the obtained XRD pattern with standard diffraction patterns, the known crystalline composition and particle lattice size could be determined. Additionally, zeta potential testing was conducted on the nanofluids to assess their stability and dispersion characteristics. The FTIR spectrum of Al_2O_3 nanoparticles is depicted in Fig. 4, which enables the identification of various bonds and their corresponding areas. Table 4 lists the known index peaks and related bonds for the tested Al_2O_3 nanoparticles. Specifically, at a wavelength of 773.42 cm^{-1}, a metal oxide bond (i.e., a bond between a metal and oxygen) can be observed, which corresponds to the bond present in Al_2O_3 [67].

Figure 5 displays the results of the FTIR analysis performed on SiO_2 nanoparticles, with the corresponding bonds for this nanoparticle listed in Table 5.

The FTIR analysis results for TiO_2 nanoparticles are presented in Fig. 6, with the corresponding bonds listed in Table 6. As per the data provided in the table, a metal oxide (Ti–O) bond can be observed at a wavelength of 809.09 cm^{-1}, which corresponds to the Ti–O bond [68, 69].

The X-ray diffraction (XRD) spectra for alumina, silica, and titania nanoparticles are illustrated in Figs. 7–9, respectively.

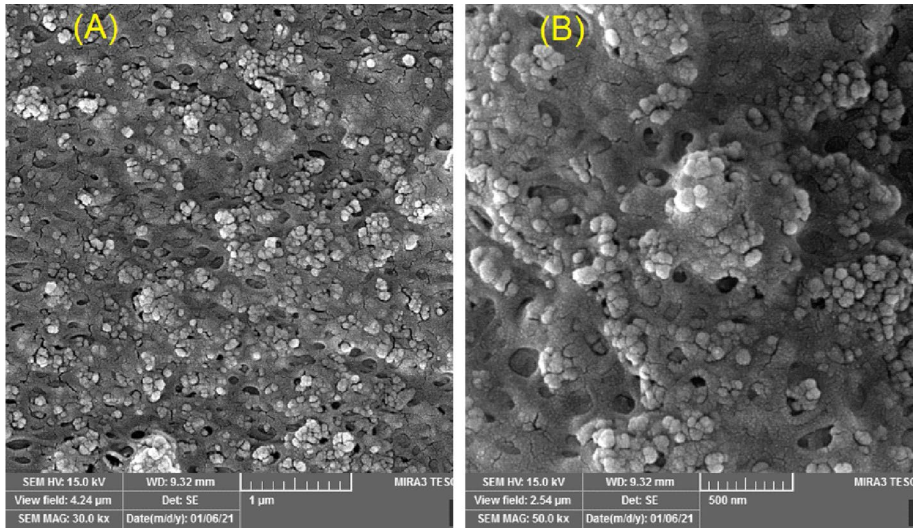

Fig. 3 FESEM images of titania (TiO_2) nanoparticles. **A** Low magnification and **B** high magnification

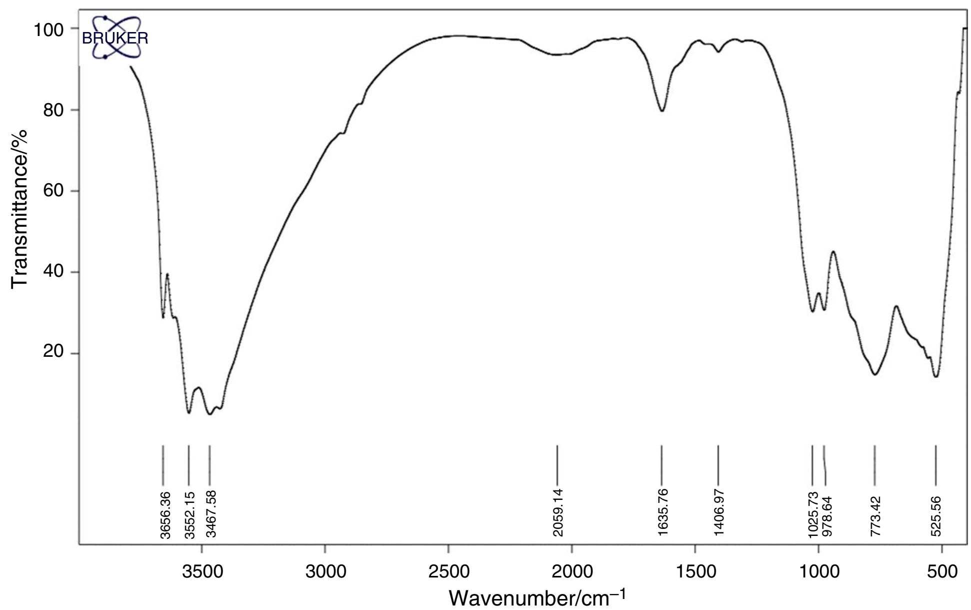

Fig. 4 FTIR spectrum of Al_2O_3 nanoparticles

Table 4 Bonds information related to Al_2O_3 nanoparticles obtained from FTIR analysis

	Wavelength/cm^{-1}	Bond type
1	3467.58, 3552.15, 3656.36	O–H
2	1635.76	Dual bond C=C
3	1406.97	Bending bond O–H
4	773.42	Al–O metal oxide bond
5	525.56	Al–O–Al

To calculate the average crystalline size of the nanoparticles, the Debye–Scherrer equation, which is represented by Eq. 1, was used [70].

$$C_s = \frac{k\lambda}{\beta \mathrm{Cos}\theta} \quad (1)$$

where C_s is the average crystalline particle (nm), k dimensionless crystal shape factor with constant value 0.94, wavelength of XRD with copper source, peak width at half maximum height (FWHM[2]) in radian, and diffraction angle (radian). Using the above relation, the particle size of the Al_2O_3 nanoparticles was 35 nm and this size was calculated for SiO_2 and TiO2 nanoparticles as 30 and 20 nm, respectively.

[2] full width at half maximum.

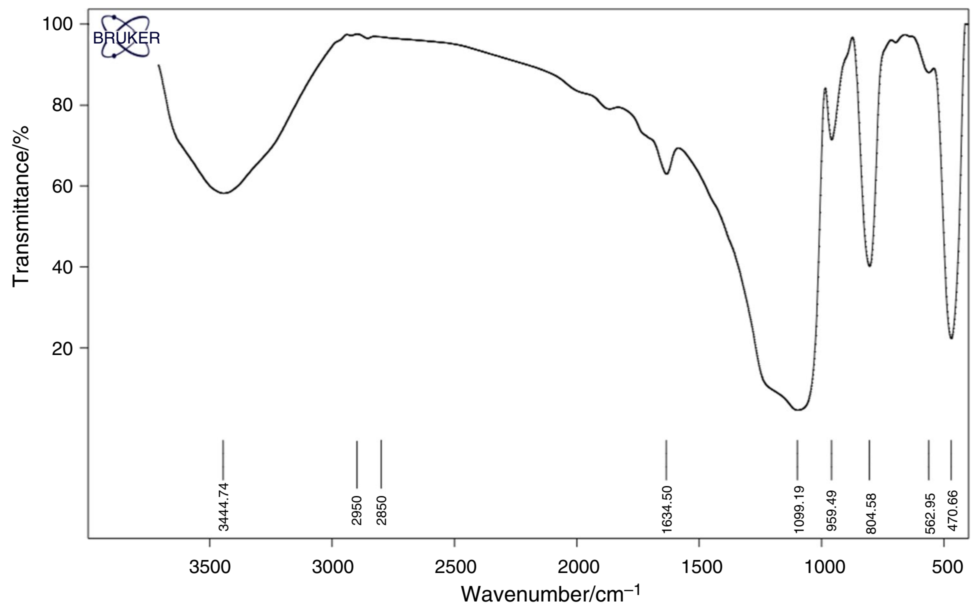

Fig. 5 FTIR spectrum of SiO_2 nanoparticles

Table 5 Bonds information related to SiO_2 nanoparticles obtained from FTIR analysis

	Wavelength/cm^{-1}	Bond type
1	3444.74	O–H
2	2950, 2850	C–H
3	1634.50	C=C
4	1099.19	C–O
5	804.58	Si–O
6	470.66	Si–O

The XRD pattern of gamma phase alumina nanoparticles conforms to the standard Al_2O_3 reference (JCPDS[3] Card 29-0063). The same pattern was observed for anatase phase titania nanoparticles with standard reference of TiO_2 (JCPDS Card 21-1272). Peaks are also seen in 25.36, 37.84, and 48.09 that match the specifications of anatase TiO_2.

Zeta potential is a measure of the electric potential difference between the surface of a particle and the surrounding fluid. It is a key indicator of the stability of colloidal

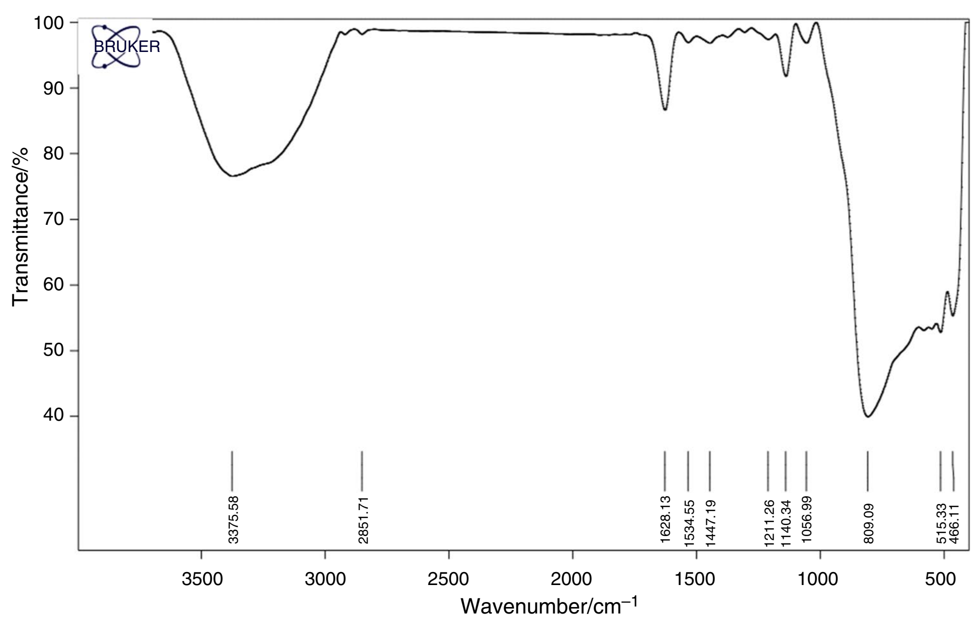

Fig. 6 FTIR spectrum of the tested TiO_2 nanoparticles

[3] Joint Committee on Powder Diffraction Standards.

Table 6 Bonds information related to TiO_2 nanoparticles obtained from FTIR analysis

	Wavelength/cm^{-1}	Bond type
1	3375.58	Tensile bond O–H
2	2950, 2851.71	C–H tensile bond
3	1140.34	The only weak bond is C–O
4	809.09	Ti–O metal oxide bond

suspensions such as nanofluids, which are composed of nanoparticles dispersed in a liquid medium. High zeta potential shows high repulsion among the nanoparticles resulting in stable suspensions. Conversely, low zeta potential values indicate weak repulsion forces among the nanoparticles leading to particles aggregation and eventual sedimentation. Zeta potential analysis was conducted on alumina, silica, and titania nanofluids to evaluate nanoparticles size and nanofluid stability a few hours after synthesis. Table 7 provides the results of the zeta potential analysis for the nanofluids. Colloids with high zeta potential values (positive or negative) are considered to be electrically stabilized, while those with low values tend to aggregate. Nanofluids exhibiting a zeta potential range of 40 to 60 mV are considered to have excellent stability [71].

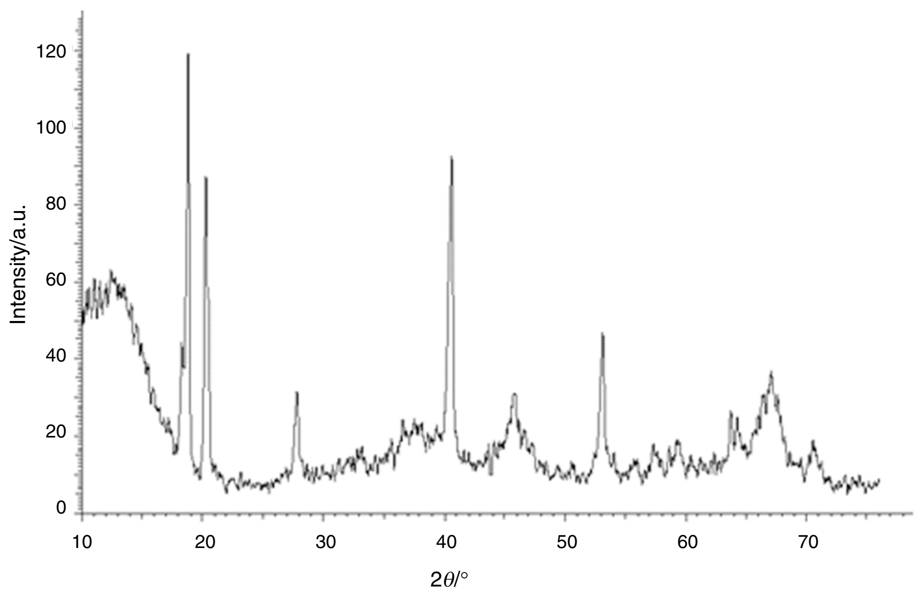

Fig. 7 XRD pattern of Al_2O_3 nanoparticle

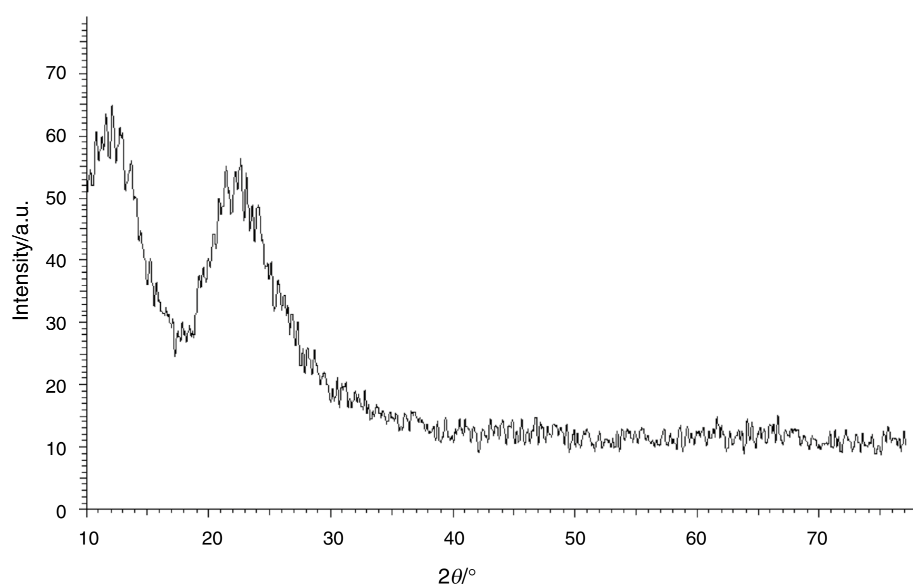

Fig. 8 XRD pattern of SiO_2 nanoparticle

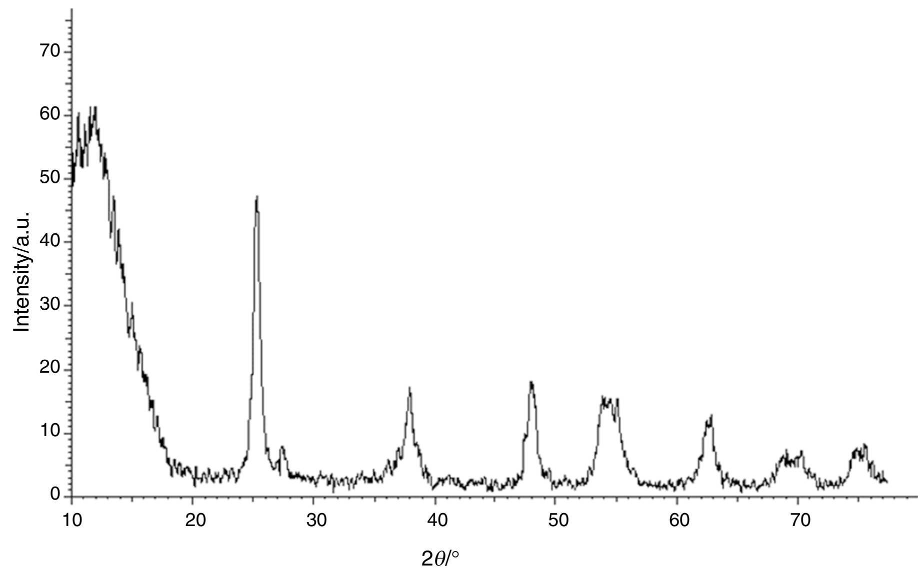

Fig. 9 XRD pattern of TiO_2 nanoparticle

Table 7 Zeta potential and DLS analysis data a few hours after nanofluid synthesis

Nanofluid	Zeta potential/mV	Particle size
Alumina	46.2	97%: 72 nm
		3%: > 100 nm
Silica	47.9	97%: 60 nm
		3%: > 100 nm
Titania	45.3	97%: 58 nm
		3%: > 100 nm

Table 8 Data related to the density of nanofluids and base fluid

Fluid	Base fluid	Alumina nanofluid	Silica nanofluid	Titania nanofluid
Density at T = 25 °C	1.00616 g mL^{-1}	1.00816 g mL^{-1}	1.0064 g mL^{-1}	1.00714 g mL^{-1}

Physical and thermophysical properties of fluids

Various instruments were used to measure the physical and thermophysical properties of the fluids, such as density, specific heat capacity, and viscosity. The density of both the base fluid and nanofluids was determined using a pycnometer, which is a device used for measuring the volume and density of small objects. In order to calculate the specific heat capacity, the base fluid and nanofluids were analyzed by DSC,[4] which is a thermal analysis technique, and is used to measure changes in the heat flow of a sample as it undergoes temperature changes. Also, Table 8 presents the fluids density. It is worth noting that for both the nanofluids and the base fluid, the density was measured at only one temperature. It is important to note that any changes in density during the heat absorption or retention phases of the experiments are likely to be negligible. In other words, although the density was measured at only one temperature, it is unlikely to have varied significantly during the experiments and therefore would not have had a significant impact on the results. According to a study by Vajjha et al., it was found that at a concentration of 1% by volume of Al_2O_3 nanofluid, there is a reduction in density of 2.51% when the temperature of the fluid increases from 0 to 50 °C. This indicates that while changes in temperature can indeed affect the density of nanofluids, such effects may be relatively small and need to be taken into account when conducting experiments or analyzing data [72].

To calculate the specific heat capacity of the fluids, the nanofluids and base fluid were analyzed by DSC. The temperature range to run DSC analyses was selected from 10 to 90 °C. At first, fluids were heated. They were then cooled from 90 to 10 °C and the resulting graphs were plotted. Finally, the specific heat capacity of the fluids was calculated by calculating the surface area below the DSC-time diagram. Table 9 presents the relevant data obtained from this analysis. Besides, Fig. 10 displays images of DSC analysis done on various fluids.

The kinematic viscosity of both the nanofluids and the base fluid was measured using a Brookfield viscometer. Shear thickening and shear thinning are two types of non-Newtonian fluid behavior that describe how a fluid's viscosity changes in response to shear stress or shear rate. Shear thickening fluids exhibit increase in viscosity when subjected to shear stress. This is due to the formation of

[4] Differential Scanning Calorimetry.

Table 9 Mean values of specific heat capacity of fluids during heating and cooling processes

Sample	Temperature range	Average heating capacity for heating	Temperature range	Average heat capacity for cooling
Alumina nanofluid	10–90	3.150	90–10	2.3
Silica nanofluid	10–90	2.95	90–10	1.9
Titania nanofluid	10–90	2.760	90–10	1.2
Base fluid	10–90	3.520	90–10	3.359

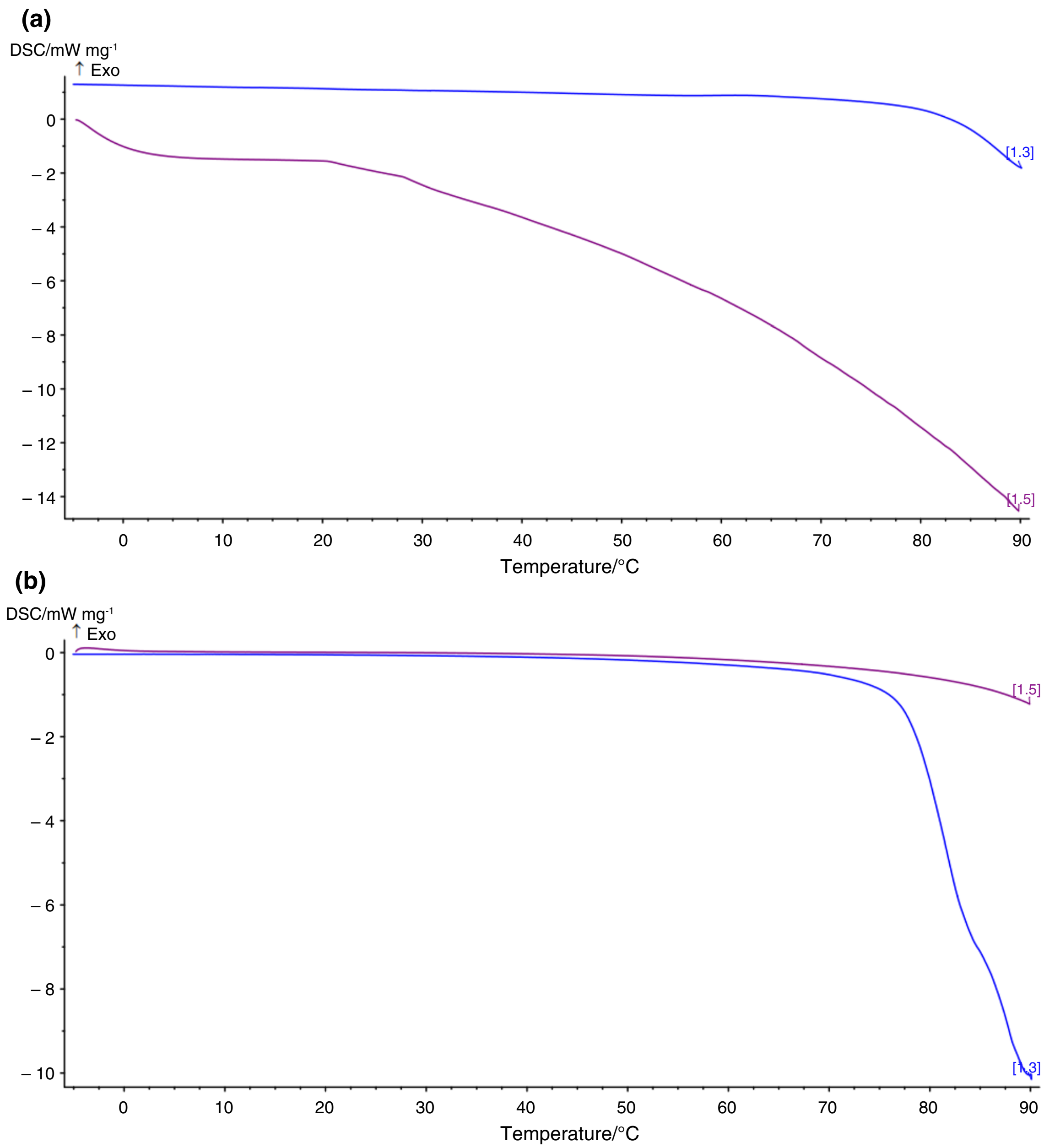

Fig. 10 DSC analysis for different fluids: **A** Alumina nanofluid, **B** silica nanofluid, **C** titania nanofluid, and **D** base fluid

temporary particle networks that resist against shear stress, resulting in a stiffening effect. Shear thinning fluids, on the other hand, exhibit a decrease in viscosity with increasing shear rate. This occurs due to the breaking down of

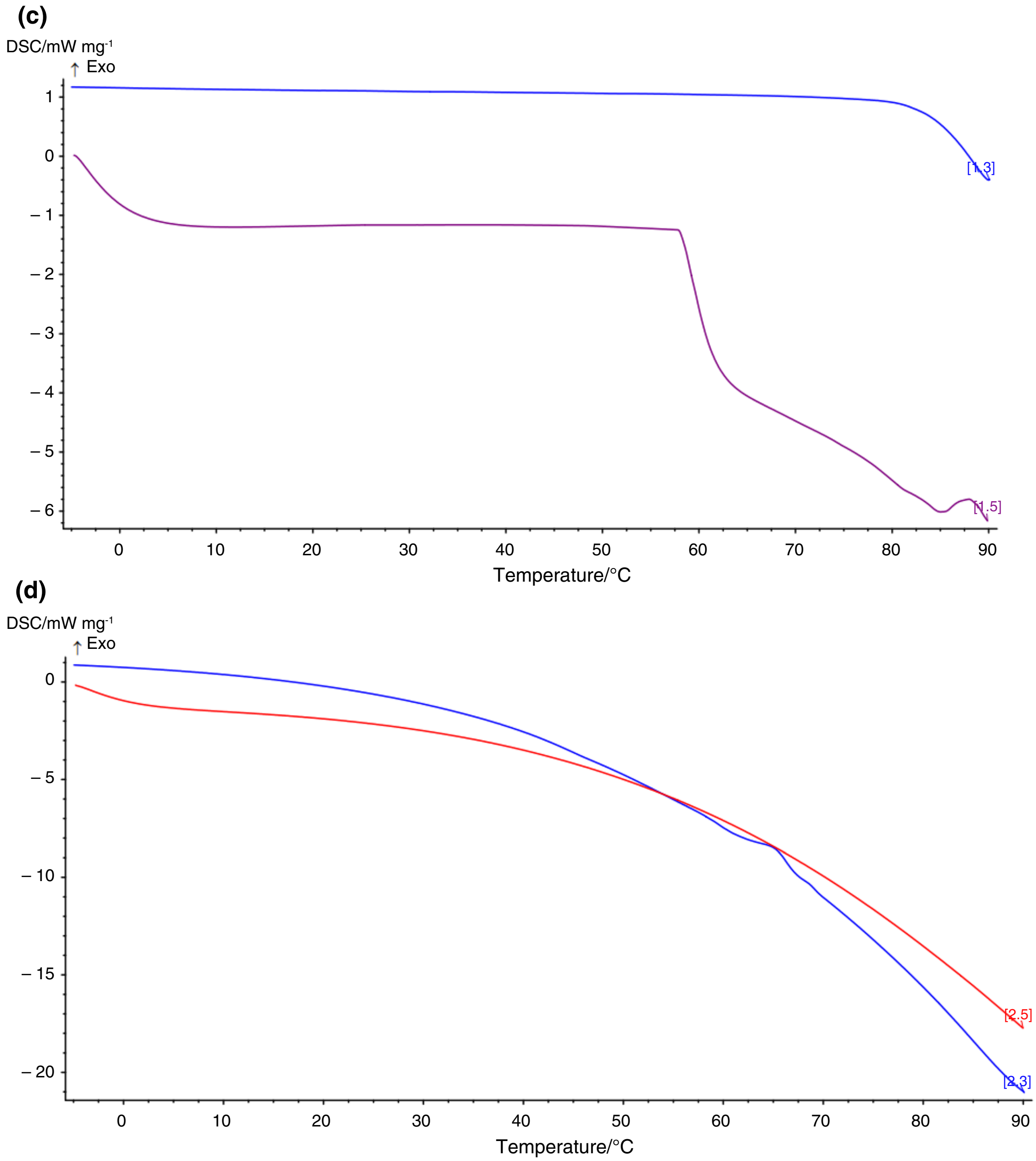

Fig. 10 (continued)

long-chain molecules or aggregates through shearing forces, leading to a more fluid-like behavior. The ability of a fluid to exhibit shear-thickening or shear-thinning behavior is dependent on various factors, including particle concentration, particle size, shape, and surface chemistry. Understanding these properties and the resulting behavior is crucial in optimizing the performance of nanofluids for specific applications. As mentioned, kinematic viscosity of the fluids was assessed via a Brookfield viscometer at various rotational speeds. The dynamic viscosity results are shown in Fig. 10. The findings reveal that as rotational velocity increased from 10 to 120 rpm at room temperature (approximately 21 °C), the viscosity of the base fluid, silica nanofluid, and alumina nanofluid decreases. However, the dynamic viscosity of TiO_2 nanofluid increases with increasing the shear rate due to TiO_2 nanofluid characteristics as a shear thickening fluid.

Figure 11 shows the dynamic viscosity changes curve for the base fluid and nanofluids at different rotational velocities. The accuracy in viscosity measurement was ± 1%.

As depicted in Fig. 11, the viscosity of the base fluid appears to be higher than that of the nanofluids. This is likely due to the increased density of the mixture when

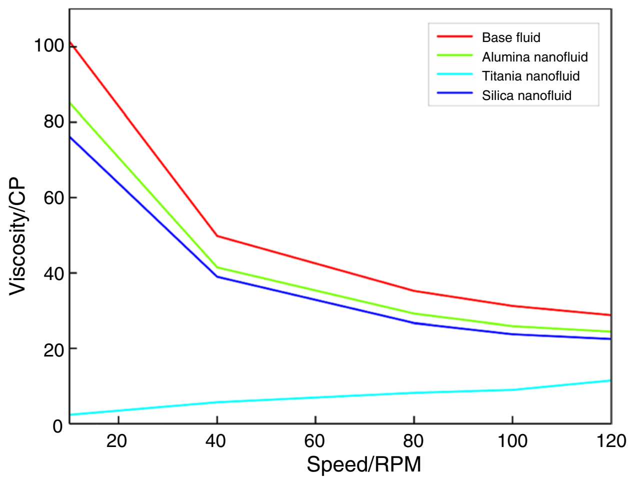

Fig. 11 Changes in the dynamic viscosity of the fluids tested at different rotational velocities

solid particles are added to the liquid. This increased density requires more force to overcome shear forces, resulting in a higher viscosity for the mixture. The comparatively high viscosity of the base fluid, as opposed to the nanofluids, may be attributed to small disturbances in the hydrogen bonding network. In completely hydrogen-bonded liquids, even minor disruptions can result in a significant reduction in viscosity. The presence of metal oxide nanoparticles within the liquid may serve to disrupt the hydrogen bonds between water molecules through chemical interactions between the surface of the nanoparticles and surrounding water molecules, resulting in reduced viscosity [73]. As temperature increases, the viscosity of the nanofluids and base fluid is expected to decrease due to the weakening of intermolecular forces at higher temperatures [74]. Therefore, during the heat absorption stage of the experiment, it is anticipated that both the nanofluids and base fluid would experience a reduction in viscosity.

Experimental setup and procedure

Experimental setup

Figure 12 illustrates the experimental setup with key components. These include a FPSC, an insulated tank, tubing system, a water pump, distilled water as the operating fluid, nanofluid/base fluid as service fluid, heat–light sources (lamps), temperature sensors, an Arduino board with associated circuitry, and a laptop.

Experimental procedure

In the designed setup, the stationary nanofluid/base fluid contained within the fixed FPSC absorbs heat from the heat–light source. This source is a lamp located at the end of an aluminum box, 31 cm away from the collector. Polyurethane foam and glass wool insulation cover the sides and back of the collector. Several types of heat–light sources can be used including tungsten, infra-red, halogen pencil, and mercury vapor lamps. The collector is filled with 760 mL of the prepared service fluid. The service fluid remains stationary inside the collector once it is injected. Inside the insulated water tank, a water pump is installed to circulate the distilled water (operating fluid) through the embedded copper tubing system inside the collector. As distilled water passes through the tubing, the operating fluid absorbs heat from distilled water. The heated operating fluid then flows back into the insulated water tank. After absorbing heat from distilled water, the copper tubes allow distilled water to flow into the collector and return to the insulated tank. The experiment is carried out by repeating and continuing this cycle. The temperature at six different points is measured

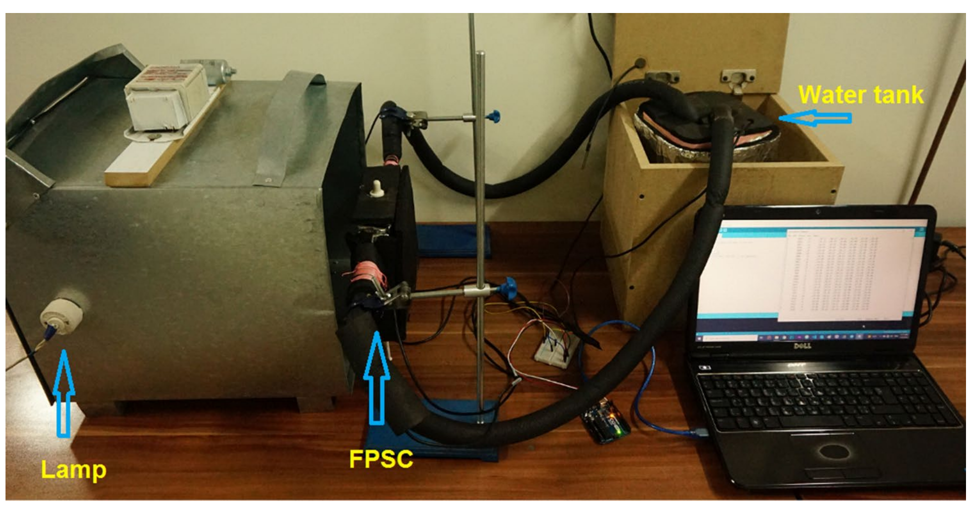

Fig. 12 Experimental setup used in the present research

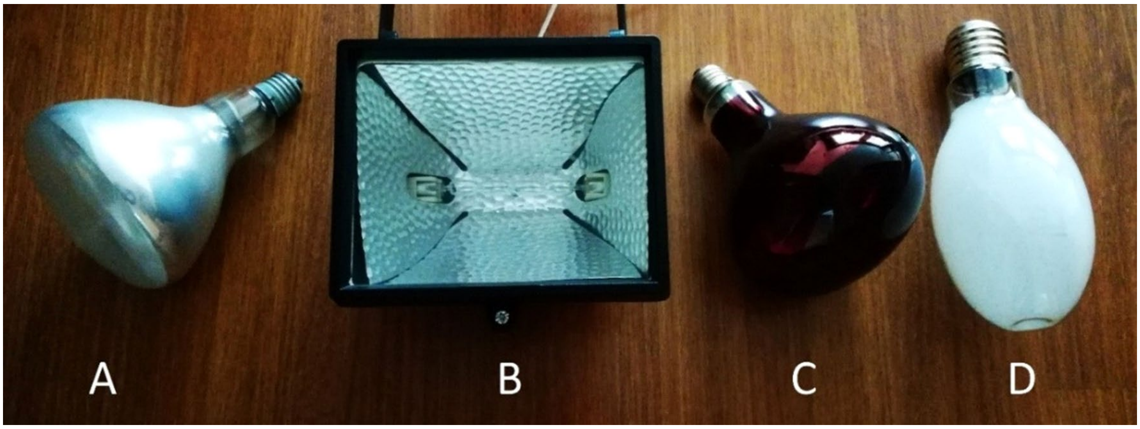

Fig. 13 Lamps used as heat–light source; **A** tungsten heat lamp, **B** halogen pencil lamp, **C** infrared lamp, and **D** mercury vapor lamp

using temperature sensors. Of these sensors, two are inside the collector, two others are in the inlet and outlet of the collector, one is inside the distilled water tank, and the last one measures the ambient temperature. The utilized temperature sensors are type DS18B20 waterproof with stainless steel probe. Before running the tests, all sensors are calibrated.

Measurements were taken and recorded every two seconds to obtain reliable data. Different types of lamps with different wavelengths and frequencies were utilized in order to simulate radiation from various heat–light reservoirs. Figure 13 displays the utilized lamps used in the experiments. The majority of the electrical energy used by lamps is spent on heat production rather than light, resulting in low light efficiency. The spectral energy distribution of the utilized lamps has a starting wavelength of 700 nm. In contrast, the sun's distribution begins at a wavelength of 300 nm. Although due to the spectral mismatch between the sun and these lamps the amount of heat absorption by service fluid and its transfer to the operating fluid will be different, this study does not aim to examine these effects. The collector was placed in a completely vertical position at a 90° angle with respect to the horizon in front of the lamps for all experiments.

The average light radiation reaching the collector surface was measured using a luxmeter. Table 10 provides the average radiation intensity values of different lamps from the light source to the collector surface. The specifications of the designed and built flat plate solar collector are listed in Table 11.

Figure 14 shows the fabricated collector before installation of the sensors and insulation. The experiments were conducted in two stages. The first stage involved a four-hour experiment, consisting of two hours of heat absorption and two hours of heat retention, while the second stage consisted of an eight-hour experiment, including four hours of heat absorption and four hours of heat retention. During the heat absorption phase, the lamp was turned on, and the service fluid absorbed radiation directly from the lamp and transferred it to the circulating water. In the heat retention phase, the lamp was turned off, but water continued to circulate inside the tubing system and storage tank. A data logger and an Arduino program were used to collect and record the data during both stages of the experiments. Figure 15 displays a schematic of the collector

Table 10 Average radiation rate reaching the collector surface center when using different lamps

Lamp	Intensity of light (lux)	Intensity of light/W m^{-2}
Tungsten heat lamp	2000	22.22
Halogen pencil lamp	950	39.58
Infra-red lamp	830	15.96
Mercury vapor lamp	715	14.3

Table 11 Specifications of the designed and built flat plate solar collector

Specifications	Dimensions
External dimensions of the collector	15×15×4 cm
Internal volume with sensors and copper tube	760 CC
Surface area exposed to heat	225 cm^2
Body thickness	4 mm
Body material	Plexiglass
Pipe material inside the collector	Copper
Diameter pipe	6.35 mm (1.4 inch)
Length of the pipe	150 cm
Type of thermal insulation	Fiberglass and elastomeric foam
Thickness of fiberglass	1 cm
Thickness of elastomeric foam	1 cm

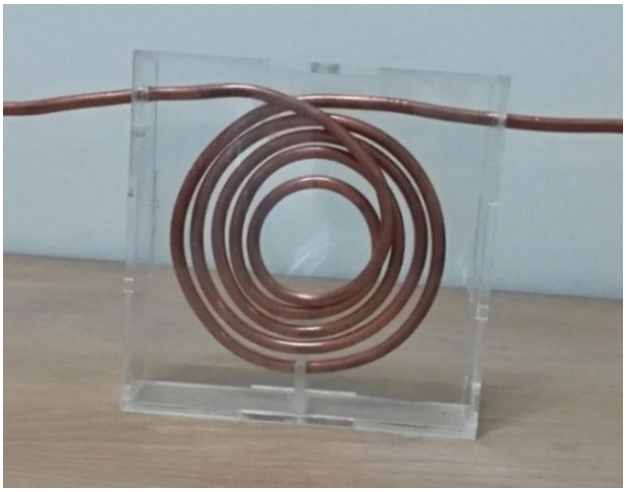

Fig. 14 View of the fabricated collector before insulating and installing the sensors

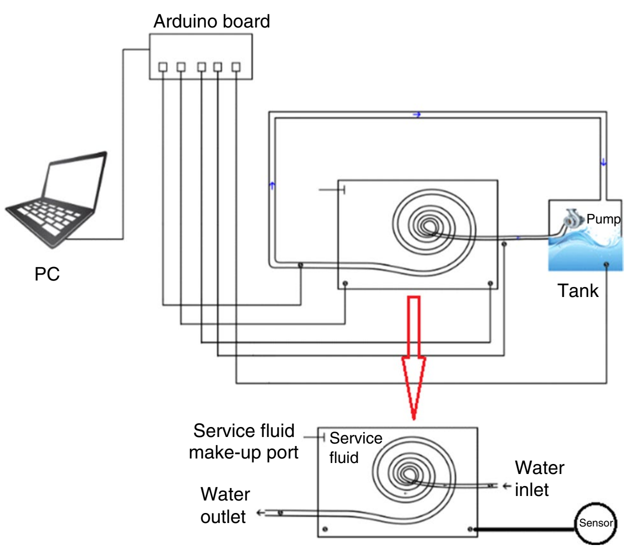

Fig. 15 Schematic of the experimental setup and data logger sets

and data logger setup that was utilized during the experiments. Each experiment was repeated three times, and all presented results are the average of those three repetitions.

Thermal efficiency calculation

Equation 2 is used to determine the amount of heat absorbed by the operating fluid [75, 76].

$$Q_{of} = \dot{m}C_p(t_o - t_i) \tag{2}$$

where Q_{of} is the amount of heat absorbed by operating fluid in W, $\dot{m}$ is the mass flow rate in kg s^{-1}, and C_p is the specific heat capacity in J kg^{-1} °C^{-1}. Also, t_o and t_i are the outlet and inlet temperatures in °C, respectively. The collector thermal efficiency can be obtained using Eq. 3 [76]:

$$\eta = \frac{Q_{of}}{A_C G} = \frac{\dot{m}C_p(t_o - t_i)}{A_C G} \tag{3}$$

where η is the collector thermal efficiency, A_C is the area of the collector surface in m^2, and G is the average light intensity arrived to the collector surface in W m^{-2} (in current study was measured using a luxmeter, MASTECH, MS6612, China). As shown in Fig. 11, in current closed system, heat is radiated from the heat source (tungsten heat lamp, halogen pencil lamp, infrared lamp and mercury vapor lamp) to the collector located at distance L. Some heat is absorbed by service fluid (Q_s), operating fluid (Q_{of}), collector body (Q_{cb}), collector tubing (Q_{ct}), and water tank body (Q_{wtb}). The total heat absorbed by collector (Q) is summation of the mentioned energies. Also, part of the heat is lost to environment mainly from collector surface by heat convection mechanism (Q_L). Other parts of the collector have been insulated carefully. Consequently, the total radiation reaching the collector surface (Q_t) can be determined using Eq. 4.

$$Q_t = Q_s + Q_{of} + Q_{cb} + Q_{ct} + Q_{wt} + Q_L \tag{4}$$

One possible way to calculate the total amount of absorbed energy is by using Eq. 5.

$$Q_{abs} = Q_s + Q_{of} + Q_{cb} + Q_{ct} + Q_{wt} \tag{5}$$

On the other hand:

$$Q_t = A_C G \tag{6}$$

In conventional FPSCs, for operating fluid Eq. 7 may also be used [76].

$$Q_{of} = A_C F_R\left[G\tau\alpha - U_L(T_i - T_a)\right] \tag{7}$$

where F_R is heating removal factor, $\tau\alpha$ is the absorption/product conversion, U_L is the general loss coefficient of the solar collector, T_i is the inlet operating fluid temperature, and T_a is the ambient temperature. However, in the current study due to the fact that the designed collectors are unconventional, and tubing inside the collectors has spiral or helical shape, some of the parameters could not be measured or calculated. Besides, there is no fin, bond, and parallel tubes in current collectors, so Eq. 7 does not attain the correct answer.

Results and discussions

Different heat–light sources

Three different nanofluids, i.e., TiO_2, SiO_2, and Al_2O_3, and base fluid as service fluid were examined using four different

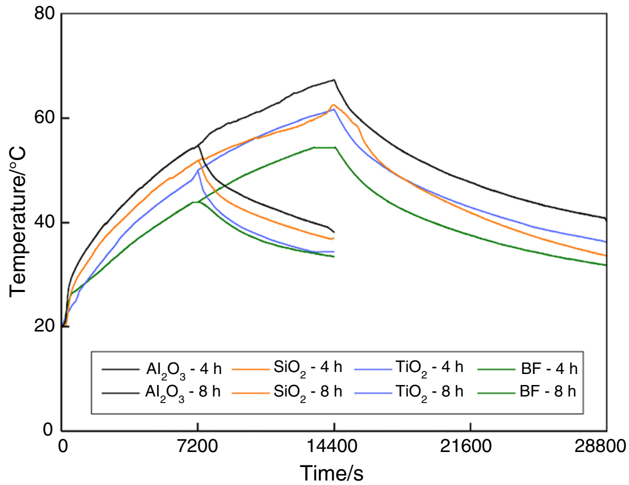

Fig. 16 Variation in temperature in time for alumina, silica, titania, and base fluid when using tungsten heat lamp in four and eight-hour experiments

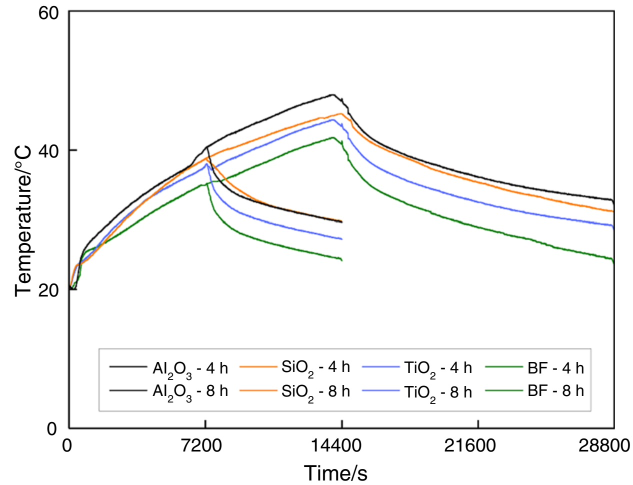

Fig. 18 Variation in temperature in time for alumina, silica, titania, and base fluid when using infrared lamp in four- and eight-hour experiments

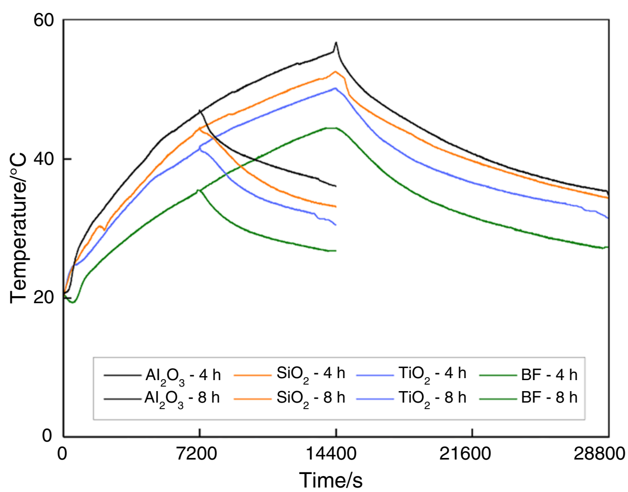

Fig. 17 Variation in temperature in time for alumina, silica, titania, and base fluid when using halogen pencil lamp in four- and eight-hour experiments

types of lamps by applying constant conditions for all experiments. Figures 15–18 show the temperature changes of the service fluid using different lamps.

According to Fig. 15, at the very early stage of the heat absorption, all the curves have the highest temperature increase rate. This is due to the significant temperature difference between the collector and the light–heat source. As time goes on, slopes become shallow. Overall, at a given moment, due to the difference in special heat capacities, Al_2O_3 nanofluid temperature has the highest temperature while the base fluid has the lowest temperature. This scenario is valid for both four- and eight-hour experiments during heat absorption and retention.

The maximum temperature of Al_2O_3 nanofluid at the end of the heat absorption stage when using tungsten heat lamp, halogen pencil bulb, infrared, and mercury vapor lamps is 67.2, 56.5, 48, and 45.8 °C, respectively. When the collector is at its maximum temperature by disconnecting the heat source, the collector begins to discharge heat with different intensities. In general, the declining slope of the curves is different than the inclining slope in the heat absorption step. This phenomenon can be attributed to the temperature difference between the collector and the environment, and to the differences in the specific heat capacities of the utilized service fluids. As the heat retention step continues, the heat dissipation slope is somewhat reduced. It can be stated that by changing the type of the service fluid, changes in the process of heat absorption and retention in the collector could be observed. According to the fact that alumina nanoparticles have higher thermal conductivity than titanium nanoparticles, using alumina nanofluid as a service fluid in collector, the heat absorption and transfer will happen better and quicker than the other service fluids.

Comparing Figs. 16–19 together, a significant difference can be predicted in the early stage of the heat retention time for both four-hour and eight-hour experiments. Based on the data presented in Fig. 19, it is evident that alumina nanofluid suffers greater heat dissipation than either the base fluid, titania, or silica nanofluid during the heat retention time. These results indicate that nanofluids lose more heat than the base fluid during the heat retention period indicating nanofluids heightened cooling abilities. This may be due, at least in part, to the nanofluids relatively reduced specific

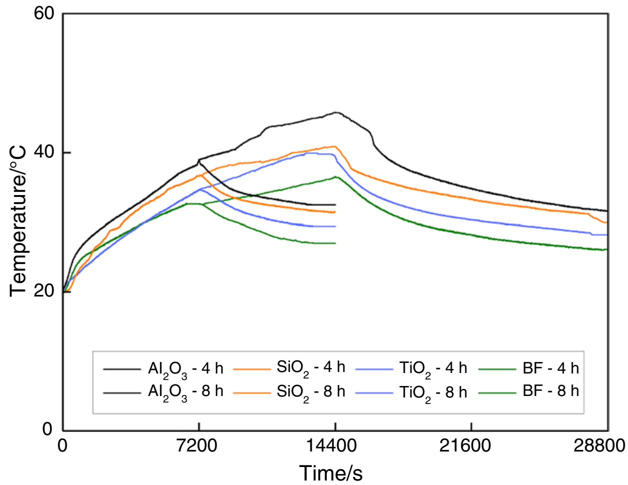

Fig. 19 Variation in temperature in time for alumina, silica, titania, and base fluid when using mercury vapor in four- and eight-hour experiments

heat capacity. Although titanium nanoparticles possess a lower heat capacity than alumina nanoparticles, which might suggest that titanium nanofluid would have a greater heat absorption rate than alumina nanofluid, the opposite is true. According to Figs. 16–19 alumina nanofluid performs better than titania in terms of heat absorption because of greater thermal conductivity. As a result, it experiences a greater increase in temperature compared to the other samples under identical experimental conditions. When comparing the results of heat absorption stages between experiments lasting four and eight hours, it is obvious that increasing the heat–light exposure time leads to a high heat absorption by both the nanoparticles and base fluid. This leads to faster cooling rate during the subsequent cooling stage. Of course, the declining slope of the curves during the heat discharge step typically differs from the inclining slope in heat absorption stage. The temperature difference between the collector and its surrounding environment, along with the differences in specific heat capacities of the service fluids, explains why the slopes of the curves during the heat absorption and discharge phases differ from one another. Alumina nanofluid is more favorable choice as service fluid for heat absorption and retains within the collector due to its better thermal conductivity in comparison to titanium and silica nanofluids.

According to the fact that titanium's heat capacity is lower than alumina's, it is expected that the titanium nanofluid shows more absorption rate than the alumina nanofluid, but due to the higher thermal conductivity of alumina than titania, alumina nanofluid has higher heat absorption. Therefore, its temperature increases more compared to the others in the experimental conditions with the same duration. By comparing the results of heat absorption stages in four and eight-hour experiments, it can be concluded that by

Table 12 Parameters used to calculate thermal efficiencies

Parameter	Value	Unit
Cp operating fluid (water)	4181	(J kg^{-1} K^{-1})
Cp Service fluid (nanofluid)		
Al_2O_3	3150	(J kg^{-1} K^{-1})
SiO_2	2950	
TiO_2	2760	
Base fluid	3520	
Cp copper (tubing)	385	(J kg^{-1} K^{-1})
Cp PMMA (collector body)	1466	(J kg^{-1} K^{-1})
Cp PE[a] (tank body)	2400	(J kg^{-1} K^{-1})
m operating fluid	2.00	Kg
m service fluid	0.76	Kg
m copper	0.195	Kg
m PMMA (collector body)	0.20	Kg
m PE (tank body)	0.150	Kg
A_c collector	0.0225	m^2
G		
Tungsten heat lamp	22.22	W m^{-2} K^{-1}
Halogen pencil lamp	39.58	
Infrared lamp	15.96	
Mercury vapor lamp	14.30	

[a]Polyethylene

increasing the duration of the stages, absorption of heat by the nanoparticles and base fluid is increased. Of course, the heat retention (cooling) rate is high when the heat absorption rate of nanofluids is high.

Thermal efficiency of the collector

In addition to the two-hour heat absorption period, the FPSC's time-averaged heat efficiencies were calculated during four-hour heat absorption periods (or eight-hour heat absorption-retention) using various fluids and lamps in three repetitions, as shown in Table 12. As mentioned earlier, thermal efficiency of the collector increases when nanofluids are used instead of the base fluid. Table 13 presents the time-averaged values, which are also the average of three replications. The experimental data suggest that using a nanofluid as a replacement for the base fluid results in a higher thermal efficiency, as indicated by the obtained results. It is evident from the results that the efficiency values for different fluids show significant variability when tested with various lamps. Consistent with the findings of the two-hour heat absorption stage, the results of the four-hour test indicate that the maximum efficiency is obtained

Table 13 Time-averaged thermal efficiency of flat plate solar collector using different nanofluids and its comparison with base fluid during two-hour and four-hour of heat absorption

Heat–light source type	Heat absorption time/min	Service fluid type	Efficiency based on Q_{of}/Q_t/%	Error/%	Efficiency based on Q_{abs}/Q_t/%	Error/%
Tungsten heat lamp	120	Base fluid	48.78	± 1.20	71.07	± 0.30
		Al_2O_3 nanofluid	67.37	± 1	96.98	± 1.02
		SiO_2 nanofluid	66.21	± 0.9	92.12	± 0.88
		TiO_2 nanofluid	64.64	± 0.45	87.58	± 0.42
	240	Base fluid	37.17	± 1.20	53.00	± 1
		Al_2O_3 nanofluid	44.72	± 1.10	63.18	± 0.32
		SiO_2 nanofluid	43.42	± 0.8	60.72	± 1.28
		TiO_2 nanofluid	42.26	± 1.30	58.18	± 0.82
Halogen pencil lamp	120	Base fluid	20.87	± 1	29.95	± 0.55
		Al_2O_3 nanofluid	27.8	± 1.20	40.64	± 0.36
		SiO_2 nanofluid	27.77	± 0.23	39.98	± 1
		TiO_2 nanofluid	27.39	± 0.61	37.00	± 0.69
	240	Base fluid	16.67	± 0.83	23.00	± 0.5
		Al_2O_3 nanofluid	19.52	± 1	27.43	± 0.57
		SiO_2 nanofluid	19.03	± 0.47	26.07	± 1.06
		TiO_2 nanofluid	18.75	± 0.55	25.08	± 0.92
Infrared lamp	120	Base fluid	38.81	± 0.19	58.14	± 0.97
		Al_2O_3 nanofluid	54.37	± 1.13	79.14	± 1.2
		SiO_2 nanofluid	52.56	± 0.44	73.81	± 0.5
		TiO_2 nanofluid	51.36	± 1.14	70.61	± 1
	240	Base fluid	31.63	± 1	43.65	± 0.6
		Al_2O_3 nanofluid	36.28	± 0.5	52.34	± 0.9
		SiO_2 nanofluid	34.06	± 1.14	48.27	± 1.02
		TiO_2 nanofluid	33.76	± 0.24	46.15	± 0.5
Mercury vapor lamp	120	Base fluid	36.78	± 1.22	54.95	± 1
		Al_2O_3 nanofluid	51.65	± 1.03	76.53	± 0.83
		SiO_2 nanofluid	50.53	± 0.47	71.45	± 0.55
		TiO_2 nanofluid	49.63	± 0.87	67.60	± 0.74
	240	Base fluid	28.21	± 0.79	39.97	± 0.35
		Al_2O_3 nanofluid	33.39	± 0.61	48.80	± 1.20
		SiO_2 nanofluid	32.49	± 0.51	46.21	± 0.79
		TiO_2 nanofluid	31.24	± 1.06	42.94	± 0.96

when using alumina nanofluid with a tungsten heat lamp, while the minimum efficiency is associated with the use of a halogen pencil lamp for the base fluid.

The experimental evidence supports the conclusion that nanofluids exhibit higher convective heat transfer compared to the base fluid, resulting in increased thermal efficiency. The findings indicate that the use of nanofluids results in a higher level of useful heat energy being obtained from the solar collector when compared to the base fluid. Based on the data obtained, it is evident that when nanofluids are used, there is a significant increase in heat absorption rate coupled with a corresponding decrease in heat loss rate. Improving the thermal properties of fluids is an innovative approach to addressing the issue of low thermal conductivity, which ultimately leads to decreased thermal efficiency in devices such as heat exchangers.

Figure 20 shows the amount of heat absorbed/lost by different parts of the collector system when using different heat–light sources including heat lamp (Fig. 20A), infrared (Fig. 20B), mercury (Fig. 20C), and pencil lamp (Fig. 20D). For all the tests Al_2O_3, nanoparticle concentration is 0.2%.

Insulation effects

Insulation plays a critical role in the efficiency of solar collectors. A well-insulated collector can minimize heat loss and effectively trap solar energy, leading to higher

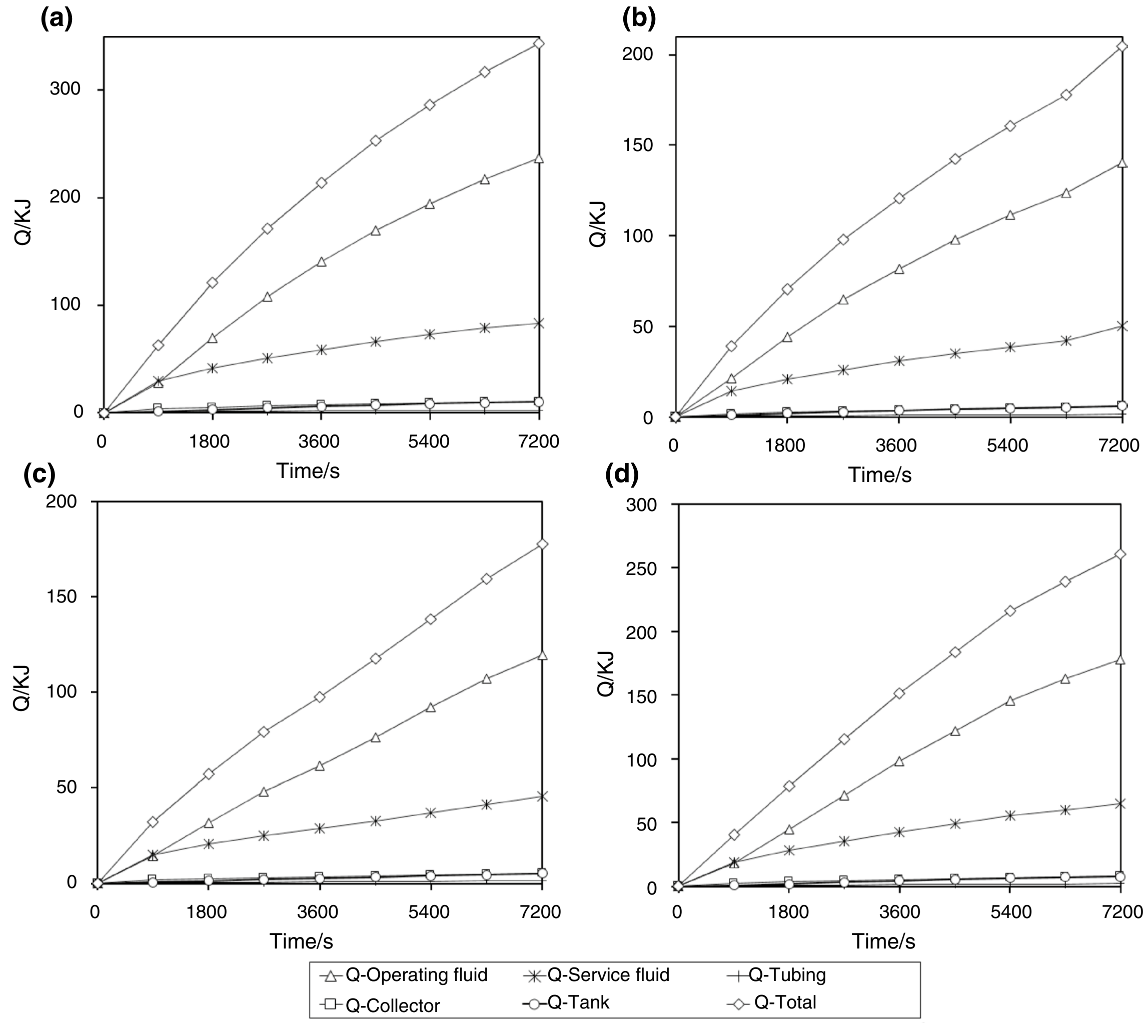

Fig. 20 Amount of heat absorbed/lost by different parts of the collector system for four-hour heat absorption-retention test when using different kinds of lamps; **A** heat lamp, **B** infrared lamp, **C** mercury vapor lamp, and **D** halogen pencil lamp

temperatures and better performance. On the other hand, poor insulation can result in significant heat loss, reducing the performance and efficiency of the solar collector. During cold weather conditions or at night, the insulation helps keep the heat inside the collector, ensuring that the stored heat is not lost to the surrounding environment. This means that the solar collector can continue to provide hot water or warm air even in the absence of sunlight. In addition, good insulation can help protect the collector from damage caused by freezing or overheating. Overall, efficient insulation is crucial for maximizing the performance of solar collectors and minimizing thermal losses, which can have a significant impact on the overall effectiveness and cost-effectiveness of the system.

Few tests were designed to examine effects of collector insulation on the heat absorption capabilities of the FPSC. To achieve this, the collector's glass wool insulation and elastomeric foam were removed, and an eight-hour test was conducted three times using alumina, silica, and titania nanofluids with a halogen pencil lamp. The results are shown in Fig. 21. As shown, for all tests, insulation results in reduced heat losses to the environment, leading to lower thermal dissipation and higher collector efficiency. In the designed experiment, the time-averaged thermal efficiency of the collector without insulation was 20%, while for the insulated collector, the efficiency raised to 23%. This efficiency increase is in accordance with literature [77].

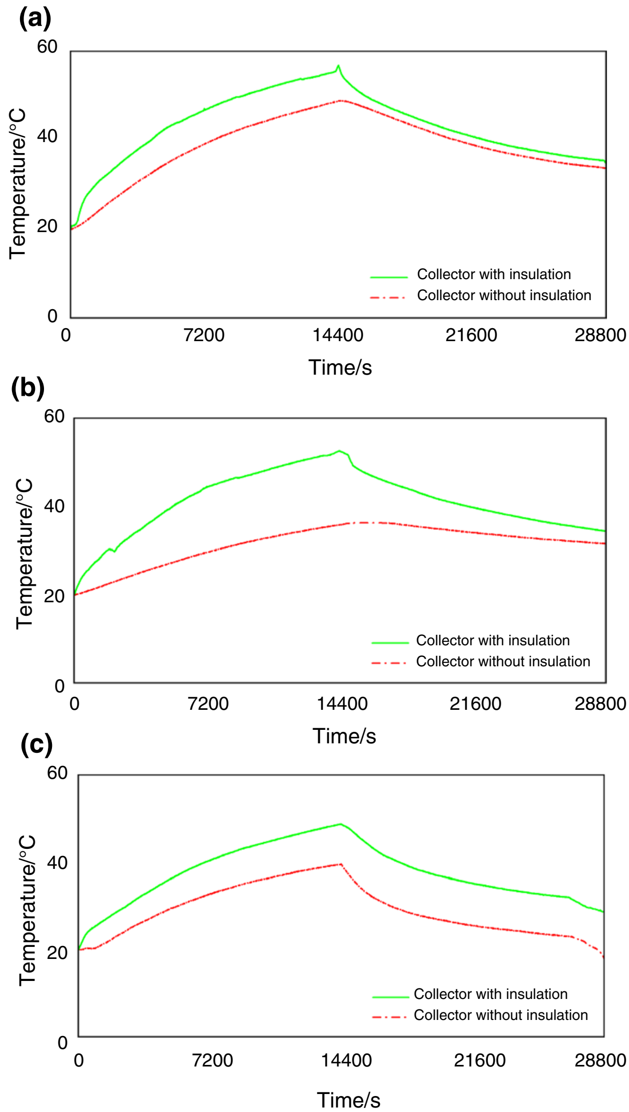

Fig. 21 Effect of collector insulation on heat absorption by nanofluids using a halogen pencil lamp in eight-hour test: **A** Alumina nanofluids, **B** silica nanofluids, and **C** titania nanofluid

Effect of SDS concentration on heat transfer

The addition of surfactant to nanofluids can have a significant impact on the stability and thermal properties of the fluid. However, it is important to note that the amount of surfactant added to the nanofluid must be carefully controlled. Excessive amounts of surfactant can lead to a reduction in thermal conductivity and other negative effects, such as increased viscosity and decreased flow rate. On the other hand, too little surfactant may result in poor stabilization of the nanoparticles, leading to particle agglomeration and settling. Overall, the influence of adding surfactant to nanofluids can be positive if the right amount is used. Careful consideration of the type and concentration of surfactant is essential to achieve optimal results in terms of nanofluid stability and thermal properties.

Several experiments were planned to investigate how the amount of SDS affects heat transfer using tungsten heat and halogen pencil lamps. In this experiment, pure distilled water and distilled water solutions containing SDS at varying volume concentrations (0.2%, 0.5%, and 1%) were utilized as service fluids. It was found that the use of pure distilled water resulted in the highest level of heat transfer, while adding surfactant into distilled water resulted in lower heat transfer. Moreover, previous findings have demonstrated that an insufficient quantity of SDS cannot offer enough coverage to generate electrostatic repulsion forces that can effectively counteract van der Waals attraction forces between particles, resulting in unstable nanofluids [78]. In contrast, using excessive amounts of SDS can have an adverse effect on the thermal characteristics of the fluid. So, an appropriate amount of surfactant for a specific application is necessary to avoid negative impacts on heat transfer and fluid stability.

Figure 22 depicts the changes in temperature for various service fluids over time when using either the tungsten heat lamp (Fig. 22A) or the halogen pencil lamp (Fig. 22B). As results show, for the same amount of received energy, pure distilled water reaches to the highest temperature, whereas the service fluid that contained 1% SDS exhibited the lowest temperature. Besides, the results showed that using distilled water as service fluid resulted in the highest amount of heat transfer. In other words, when distilled water containing 0.2%, 0.5%, and 1% SDS was used, heat transfer decreased with increasing SDS content.

Conclusions

The present study aimed to investigate the effect of different heat–light sources on the thermal efficiency of a flat plate solar collector. Four types of lamps, including tungsten heat lamp, halogen pencil lamp, infrared lamp, and mercury vapor lamp, were utilized as thermal radiation sources in this study. During the experiments, the thermal behavior of the prepared nanofluids in the flat plate solar collector was investigated in two stages: heat absorption with a duration of 120 and 240 min and heat retention with the same duration.

- Interestingly, the results of the 120-min heat absorption experiment demonstrated a higher efficiency compared to that of the 240-min experiment.
- Replacing the base fluid with a nanofluid is known to enhance heat transfer performance. The findings of the study validated that various types of nanofluids can have distinct impacts on the thermal efficiency of solar collectors.

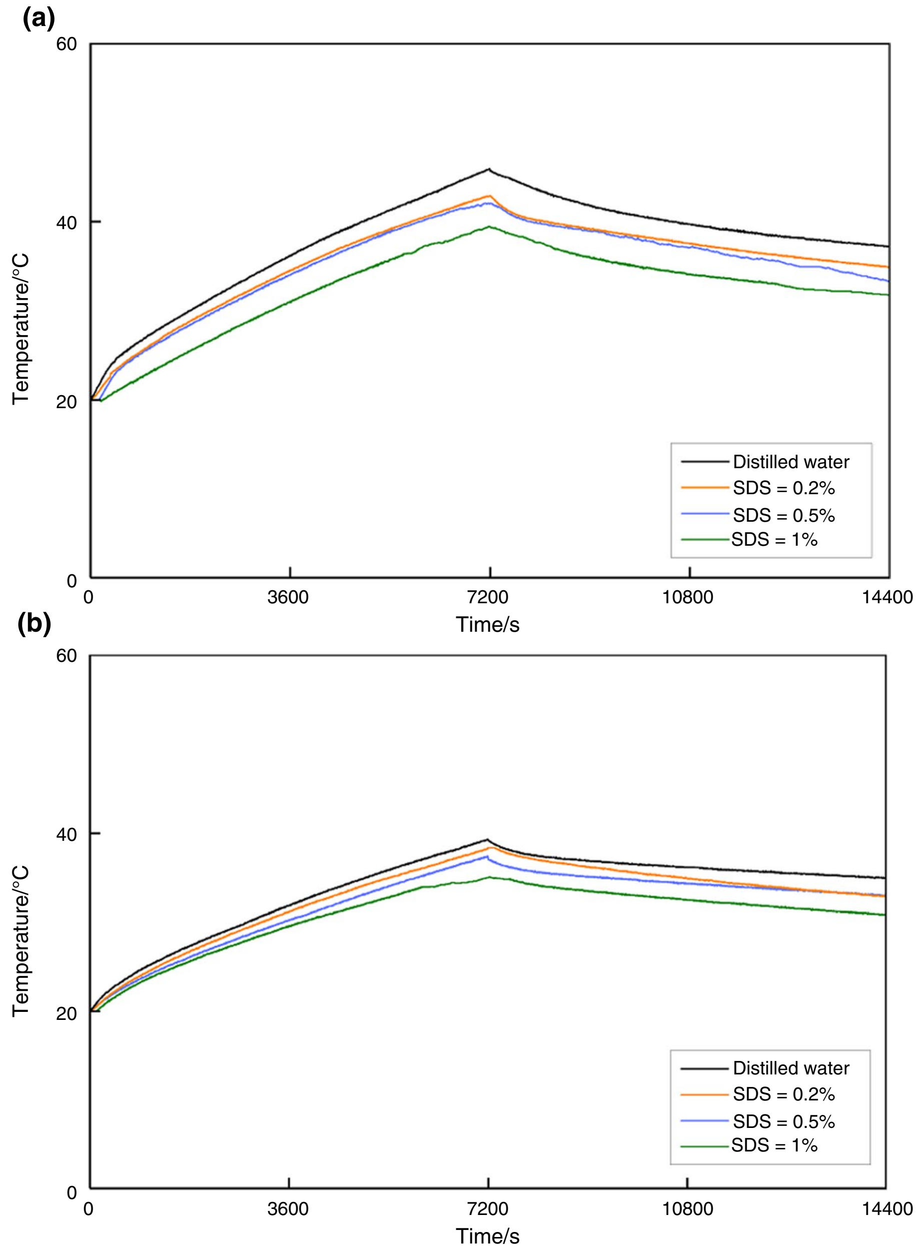

Fig. 22 Variation in different service fluids' temperature during the experiment when the heat–light source is: **A** Tungsten heat lamp, **B** halogen pencil lamp

- As per the experimental results, the collector utilizing a tungsten heat lamp demonstrated the highest thermal efficiency among all the tested heat–light sources.
- The efficiency values for a 120-min heat absorption duration were found to be 67.37% for Al_2O_3 nanofluid, 66.21% for SiO_2 nanofluid, 64.64% for TiO_2 nanofluid, and 48.78% for the base fluid when using a tungsten heat lamp.
- During the heat absorption duration of 240 min, the corresponding efficiency values for a tungsten heat lamp were 44.72% for Al_2O_3 nanofluid, 43.42% for SiO_2 nanofluid, 42.26% for TiO_2 nanofluid, and 37.17% for the base fluid.
- According to the results, the highest thermal efficiency for the FPSC was achieved when using a tungsten heat lamp with 0.2% mass-volume Al_2O_3 nanofluid.
- Comparing different nanofluids, it was found that alumina nanofluid exhibited the highest energy absorption and transmission rate to the operating fluid as compared to silica and titania nanofluids. It has been observed that nanofluids exhibit enhanced heat transfer characteristics compared to conventional fluids such as water, ethylene glycol, and oils, especially in extraterrestrial environments. One of the main reasons for the significant increase in thermal conductivity exhibited by nanoflu-

ids is the presence of suspended particles of nanoscale dimensions within the base fluid.

- One key observation from the study is that fluids containing nanoparticles have a greater capacity to absorb and retain thermal energy compared to their corresponding base fluids. Another key reason for the improved thermal absorption and retention capabilities of nanofluids is the direct absorption of photons by nanoparticles, particularly in the case of (Al_2O_3, SiO_2 and TiO2) nanoparticles. These nanoparticles have a wide bandgap, which makes it capable of absorbing UV light and converting it into heat energy. When dispersed in a fluid medium, these nanoparticles can absorb a significant portion of the incoming radiation, converting it into thermal energy and increasing the overall efficiency of the collector. This mechanism of direct photon absorption by nanoparticles is a unique advantage of nanofluids over conventional fluids and can provide a substantial boost to their thermal performance. Besides, the other factor that contributes to the improved thermal performance of nanofluids is the dispersion of light by nanoparticles. By increasing the dispersion of light in the fluid medium, the length of the path that light travels through the fluid can be extended, causing more light to remain inside the fluid and increasing heat absorption. This effect is especially notable in fluids containing nanoparticles with high refractive indices, which can scatter and absorb light more effectively than the base fluid alone. The combined effects of direct photon absorption and light dispersion by nanoparticles can lead to significant improvements in the thermal properties of nanofluids, making them an attractive option for enhancing the efficiency of solar collectors and other thermal systems.

Generally, because of several factors, such as increased heat capacity and thermal conductivity of nanofluids, their ability to reduce convection losses, and the enhanced dispersion of light by nanoparticles, nanofluids are able to retain thermal energy for more extended periods, making them a potentially valuable technology for improving the performance and efficiency of solar collectors and other thermal systems. There are several potential avenues for future studies aimed at improving and increasing the efficiency of flat plate collectors. Some possible approaches could include exploring different types of nanofluids or utilizing other advanced heat transfer fluids, incorporating novel materials into the collector design to enhance thermal insulation or increase absorption of solar radiation, optimizing the overall geometry and layout of the collector system, and evaluating new fabrication techniques or manufacturing processes that enable more precise and cost-effective production of the collectors. More researches could be done to investigate how the operation and performance of these collectors can be optimized in different operating conditions, such as extreme temperatures, high humidity, or low light environments. Evaluating changes in the performance of collectors by modifying their dimensions and utilizing various absorbent plates can aid in identifying significant factors that impact the absorption rate and thermal efficiency of the collectors. These could help the development of more efficient flat plate collector designs in the future.

Author contributions MA involved in data curation, investigation, visualization, writing—reviewing and editing. MA took part in supervision, conceptualization, methodology, analysis, writing—reviewing and editing. MM involved in supervision, conceptualization, analysis.

Funding The authors declare no financial interest or personal relationship with a third party.

References

1. Kalogirou SA. Solar energy engineering: processes and systems. Berlin: Academic Press; 2013.
2. Pandey KM, Chaurasiya R. A review on analysis and development of solar flat plate collector. Renew Sustain Energy Rev. 2017;67:641–50.
3. Otanicar T, Phelan P, Prasher RS, Rosengarten G, Taylor RA. Nanofluid-based direct absorption solar collector. J Renew Sustain Energy. 2010;2: 033102.
4. Choi SUS, Eastman J. Enhancing thermal conductivity of fluids with nanoparticles in development and applications of non-newtonian flows. Argonne National Lab; 1995. p. 99–105.
5. Wang XQ, Majumdar AS. Heat transfer characteristics of nanofluids: a review. Int J Therm Sci. 2007;46:1–19.
6. Prasher RS, Phelan PE. Modeling of radiative and optical behavior of nanofluids based on multiple and dependent scattering theories, Paper No. IMECE2005–80302, ASME International Mechanical Engineering Congress & Exposition. 2005.
7. Chicea D. Coherence light scattering on nanofluids: computer simulation results. Appl Opt. 2008;47:1434–42.
8. Khlebtsov NG, Trachuk LA, Melnikov AG. The effect of the size, shape and structure of metal nanoparticles on the dependence of their optical properties on the refractive index of a disperse medium. Opt Spectrosc. 2005;98:77–83.
9. Tyagi H, Phelan P, Prasher R. Predicted efficiency of nanofluid-based direct absorption solar receiver. Proceedings ES2007, Energy Sustainability, Long Beach, California. 2007.
10. Eastman JA, Choi SUS, Li S, Yu W, Thompson LJ. Anomalously increased effective thermal conductivities of ethylene glycol-based nanofluids containing copper nanoparticles. Appl Phys Lett. 2001;78(6):718–20.
11. Kim P, Shi L, Majumdar A, McEuen PL. Thermal transport measurements of individual multiwalled nanotubes. Phys Rev Lett. 2001;87:215502-1-215502–4.
12. Natarajan E, Sathish R. Role of nanofluids in solar water heater. Int J Adv Manuf Technol 2009.
13. Choi SUS, Zhang ZG, Yu W, Lockwood FE, Grulke EA. Anomalous thermal conductivity enhancement in nanotube suspensions. Appl Phys Lett. 2001;79(14):2252–4.

14. Assael MJ, Chen CF, Metaxa I, Wakeham WA. Thermal conductivity of suspensions of carbon nanotubes in water. Int J Thermophys. 2004;25(4):971–85.
15. Wang XQ, Mujumdar AS. Heat transfer characteristics of nanofluids: a review. Int J Therm Sci. 2007;46:1–19.
16. Masuda H, Ebata A, Teramae K, Hishinuma N. Alteration of thermal conductivity and viscosity of liquid by dispersing ultra-fine particles (dispersion of g- Al_2O_3, SiO_2 and TiO_2 ultra-fine particles). Netsu Bussei (Japan). 1993;7:227–33.
17. Grimm A. Powdered aluminum-containing heat transfer fluids. German patent DE. 1993;4131516:A1.
18. Veeranna S, Lakshmi NS. Al_2O_3-based nanofluids: a review. Nanoscale Res Lett. 2011;6:456.
19. Eastman JA, Choi SUS, Li S, Thompson LJ, Lee S. Enhanced thermal conductivity through the development of nanofluids. Mater Res Soc 1997;457.
20. Taylor RA, Phelan PE, Otanicar TP, Adrian R, Prasher R. Nanofluid optical property characterization: towards efficient direct absorption solar collectors. Nanoscale Res Lett. 2011;6:225.
21. Arthur O, Karim MA. An investigation into the thermos-physical and rheological properties of nanofluids for solar thermal applications. Renew Sustain Energy Rev. 2016;55:739–55.
22. Azmi WH, Sharma KV, Mamat R, Najafi G, Mohamad MS. The enhancement of effective thermal conductivity and effective dynamic viscosity of nanofluids: a review. Renew Sustain Energy Rev 2016.
23. Das SK, Putra N, Thiesen P, Roetzel W. Temperature dependence of thermal conductivity enhancement for nanofluids. J Heat Transfer. 2003;125:567–74.
24. Ding Y, Wen D. Experimental investigation into convective heat transfer of nanofluids at the entrance region under laminar flow condition. Int J Heat Mass Transf. 2004;47:5181.
25. Eastman JA, Choi SUS, Li S, Yu W, Thompson LJ. Anomalously increased effective thermal conductivities of ethylene glycol based nanofluids containing copper nanoparticles. Appl Phys Lett. 2001;78(6):718–20.
26. He Q, Zeng Sh, Wang Sh. Experimental investigation on the efficiency of flat-plate solar collectors with nanofluids. Appl Therm Eng. 2015;88:165–71.
27. Elsheikh AH, Sharshir SW, Mostafa ME, Essa FA, Ali MK. Applications of nanofluids in solar energy: a review of recent advances. Renew Sustain Energy Rev. 2017;82:3483–502.
28. Jang SP, Choi SUS. Role of Brownian motion in the enhanced thermal conductivity of nanofluids. Appl Phys Lett. 2004;84:4316–8.
29. Xie H, Li Y, Yu W. Intriguingly high convective heat transfer enhancement of nanofluid coolants in laminar flows. Phys Lett A. 2010;374:2566–8.
30. Li XF, Zhu DS, Wang XJ, Wang N, Gao JW, Li H. Thermal conductivity enhancement dependent PH and chemical surfactant for Cu-H2O nanofluids. Thermochim Acta. 2008;469(1):98–103.
31. Yousefi T, Veysi F, Shojaeizadeh E, Zinadini S. An experimental investigation on the effect of Al_2O_3-H_2O nanofluid on the efficiency of flat-plate solar collectors. Renew Energy. 2012;39:293–8.
32. Otanicar TP, Phelan PE, Golden JS. Optical properties of liquids for direct absorption solar thermal energy systems. Sol Energy. 2009;83:969–77.
33. Nagarajan PK, Subramani J, Suyambazhahan S, Sathyamurthy R. Nanofluids for solar collector applications: a Review. In: The 6th international conference on applied energy-ICAE2014, Energy Procedia; 2014;61:2416–2434.
34. Muhammad MJ, Muhammad IA, Che Sidik NA, Muhammad Yazid MNAW. Thermal performance enhancement of flat-plate and evacuated tube solar collectors using nanofluid: a review. Int Common Heat Mass Transfer. 2016;76:6–15.
35. Choi SUS. Metallic nanofluids research can lead to cooler engines. Transportation Technology R&D Center, TechBrief. 2007.
36. Faizal M, Saidur R, Mekhilef S, Alim MA. Energy, economic and environmental analysis of metal oxides nanofluid for flat-plate solar collector. Energy Convers Manage. 2013;76:162–8.
37. Kameya Y, Hanamura K. Enhancement of solar radiation absorption using nanoparticles suspension. Sol Energy. 2011;85:299–307.
38. Han D, Meng Z, Wu D, Zhang C, Zhu H. Thermal properties of carbon black aqueous nanofluids for solar absorption. Nanoscale Res Lett. 2011;6:457.
39. Hordy N, Rabilloud D, Meunier JL, Coulombe S. High temperature and long-term stability of carbon nanotube nanofluids for direct absorption solar thermal collectors. Sol Energy. 2014;105:82–90.
40. Singh RN, Dilipbhai SD, Rajput D, Kumar Sharm Sh. Performance analysis of flat plate solar collector using Al_2O_3/distilled water nanofluid: an experimental investigation. Mater Today Proc. 2019;10:52–9.
41. Zamzamian A, KeyanpourRad M, KianiNeyestani M, Tajik J-A. An experimental study on the effect of Cu-synthesized/EG nanofluid on the efficiency of flat-plate solar collectors. Renew Energy. 2014;71:658–64.
42. Kilic F, Menlik T, Sozen A. Effect of titanium dioxide/water nanofluid use on thermal performance of the flat plate solar collector. Sol Energy. 2018;164:101–8.
43. Tong Y, Lee H, Kang W, Cho H. Energy and exergy comparison of a flat-plate solar collector using water, Al_2O_3 nanofluid, and CuO nanofluid. Appl Therm Eng. 2019;159: 113959.
44. Ahmadlouydarab M, Ebadolahzadeh M, Muhammad-Ali H. Effects of utilizing nanofluid as working fluid in a lab-scale designed FPSC to improve thermal absorption and efficiency. Phys A Stat Mech Appl. 2020;540: 123109.
45. Qi H, Zhang Y, Wang Q, Wang F, Hussein AK, Arıcı M, Li D. Experimental investigation of optical properties of oily sewage with different pH environment. Optik. 2019.
46. Shukla KN, Koller TM, Rausch MH, Fröba AP. Effective thermal conductivity of nanofluids: a new model taking into consideration Brownian motion. Int J Heat Mass Transf. 2016;99:532–40.
47. Merkin JH, Pop I, Lok YY, Grosan T. Similarity solutions for the boundary layer flow and heat transfer of viscous fluids, nanofluids, porous media, and micropolar fluids. Academic Press; 2021.
48. Yang Q, Ye L, Du H, Zhang Z, Huang X, Xu J. Effect of nanoparticle concentration on physical and heat-transfer properties and evaporation characteristics of graphite/*n*-decane nanofluid fuels. ACS Omega. 2022;7(4):3284–92.
49. Upman KK, Srivastava A. Study on parameters of thermal conductivity enhancement in oxide nanofluids. Int J Eng Manag Sci 2014;1(12).
50. Rashmi W, Ismail AF, Sopyan I, Jameel AT, Yusof F, Khalid M, Mubarak NM. Stability and thermal conductivity enhancement of carbon nanotube nanofluid using gum Arabic. J Exp Nanosci. 2011;6(6):567–79.
51. Wang X, Xu X, Choi SUS. Thermal conductivity of nanoparticle-fluid mixture. J Thermophys Heat Transfer. 1999;13:474–80.
52. Phelan PE, Prasher RS, Rosengarten G, Taylor RA. Nanofluid-based direct absorption solar collector. J Renew Sustain Energy. 2010;2: 033102.
53. Sabaghan A, Edalatpour M, Charjouei MM, Roohi E, Niazmand H. Nanofluid flow and heat transfer in a microchannel with longitudinal vortex generators: two-phase numerical simulation. Appl Therm Eng. 2016;100:179–89.

54. Amina B, Miloud A, Samir L, et al. Heat transfer enhancement in a parabolic trough solar receiver using longitudinal fins and nanofluids. J Thermal Sci. 2016;25:410–7.
55. Gorji TB, Ranjbar AA. Thermal and exergy optimization of a nanofluid-based direct absorption solar collector. Renew Energy. 2017;106:274–87.
56. Aberoumand S, Ghamarib Sh, Shabani B. Energy and exergy analysis of a photovoltaic thermal (PV/T) system using nanofluids: An experimental study. Sol Energy. 2018;165:167–77.
57. Chen G, Su Y, Jiang D, Pan L, Li S. An experimental and numerical investigation on a paraffin wax/graphene oxide/carbon nanotubes composite material for solar thermal storage applications. Appl Energy. 2020;264: 114786.
58. Parsa SM, Yazdani A, Aberoumand H, Farhadi Y, Ansari A, Aberoumand S, Karimi N, Afrand M, Cheraghian G, Muhammad AH. A critical analysis on the energy and exergy performance of photovoltaic/thermal (PV/T) system: the role of nanofluids stability and synthesizing method. Sustain Energy Technol Assess. 2022;51: 101887.
59. Islam S, Furuta H. Recent development of carbon-nanotube-based solar heat absorption devices and their application. Nanomaterials. 2022;12:3871.
60. Kazaz O, Karimi N, Kumar S, Falcone G, Paul MC. Enhanced sensible heat storage capacity of nanofluids by improving the photothermal conversion performance with direct radiative absorption of solar energy. J Mol Liquids. 2023;372:121182.
61. Meibodi SS, Kianifar A, Mahian O, Wongwises S. Second law analysis of a nanofluid-based solar collector using experimental data. J Therm Anal Calorim. 2016;126:617–25.
62. Said Z, Arora S, Bellos E. A review on performance and environmental effects of conventional and nanofluid-based thermal photovoltaics Panel. Renew Sustain Energy Rev. 2018;94:302–16.
63. Gupta M, Singh V, Kumar S, Kumar S, Dilbaghi N, Said Z. Up to date review on the synthesis and thermophysical properties of hybrid nanofluids. J Clean Prod 2018.
64. Ghodbane M, Said Z, Hachicha AA, Boumeddane B. Performance assessment of linear Fresnel solar reflector using MWCNTs/DW nanofluids. Renew Energy 2019.
65. Ehyaei M, Ahmadi A, Assad MEH, Hachicha A, Said Z. Energy, exergy and economic analyses for the selection of working fluid and metal oxide nanofluids in a parabolic trough collector. Sol Energy. 2019;187:175–84.
66. Alawi OA, Kamar HM, Mallah AR, Mohammed HA, Kazi SN, Che Sidik NA, Najafi GH. Nanofluids for flat plate solar collectors: fundamentals and applications. J Clean Prod. 2021;291: 125725.
67. Romero TR, Santoyo VR, Moncada SD, Martínez RM. Effect of aluminum precursor on physicochemical properties of Al2O3 by hydrolysis/precipitation method. Nova Scientia. 2018;10(1):83–99.
68. Leon A, Reuquen P, Garín C, Segura R, Vargas P, Zapata P, Orihuela PA. FTIR and Raman characterization of TiO_2 nanoparticles coated with polyethylene glycol as carrier for 2-methoxyestradiol. Appl Sci. 2017;7:49.
69. Al-Amin M, ChandraDey S, Rashid TU, Ashaduzzaman M, Shamsuddin SM. Solar assisted photocatalytic degradation of reactive azo dyes in presence of anatase titanium dioxide. Int J Latest Res Eng Technol. 2016;2(3):14–21.
70. Cullity BD. Elements of x-ray diffraction. 2nd ed. Massachusetts: Addison-Wesley Publishing Co Inc; 1978. p. 284–8.
71. Mukherjee S, Paria S. Preparation and stability of nanofluids-a review. IOSR J Mech Civ Eng. 2013;9(2):63–9.
72. Vajjha RS, Das DK, Mahagaonkar BM. Density measurement of different nanofluids and their comparison with theory. Sci Technol. 2009;27:612–24.
73. Suganthi KS, Leela Vinodhan V, Rajan KS. Heat transfer performance and transport properties of ZnO–ethylene glycol and ZnO–ethylene glycol–water nanofluid coolants. Appl Energy 2014.
74. Suganthi KS, Radhakrishnan AK, Anusha N, Rajan KS. Influence of nanoparticle concentration on thermo-physical properties of CuO-Propylene Glycol nanofluids. J Nanosci Nanotechnol. 2014;14:4602–7.
75. Duffie JA, Beckman WA. Solar engineering of thermal processes. New York: Wiley; 2006. p. 240–307.
76. Akbarzadeh A, Ahmadlouydarab M, Niaei A. Capabilities of α-Al2O3, γ-Al_2O_3, and bentonite dry powders used in flat plate solar collector for thermal energy storage. Renew Energy. 2021;173:704–20.
77. Mapa LDPP, Mendes BDM, Bortolaia LA, Leal EM. Study of the project parameters influence in the performance of solar collectors. Int J Heat Technol. 2019;37(1):313–21.
78. Kumar RS, Chaturvedi KR, Iglauer S, Trivedi J, Sharma T. Impact of anionic surfactant on stability, viscoelastic moduli, and oil recovery of silica nanofluid in saline environment. J Petrol Sci Eng. 2020;195: 107634.